Supporting Information for

Dynamic changes of optical and chemical properties of tar ball aerosols by atmospheric photochemical aging

Chunlin Li,[†] Quanfu He,[†] Julian Schade,[‖] Johannes Passig,[‖,⊥] Ralf Zimmermann,[‖,⊥] Alexander Laskin,[§] and Yinon Rudich[†,*]

[†]Department of Earth and Planetary Sciences, Weizmann Institute of Science, Rehovot 76100, Israel

[‖]Joint Mass Spectrometry Centre, University of Rostock, Dr.-Lorenz-Weg 2, 18059 Rostock, Germany

[⊥]Joint Mass Spectrometry Centre, Cooperation Group 'Comprehensive Molecular Analytics' (CMA), Helmholtz Zentrum München, Ingolstädter Landstrasse 1, 85764 Neuherberg, Germany

[§]Department of Chemistry, Purdue University, West Lafayette, Indiana 47907, United States

Correspondence to: Yinon Rudich (yinon.rudich@weizmann.ac.il)

Contents

1. Tar ball aerosol size distribution at downstream of the OFR

Tar ball particles were generated via TSI atomizer, and concentration of tar ball particles was mediated in the OFR before these aerosols being photochemically oxidized. Polar, nonpolar, and mixture tar ball particles present similar size distributions.

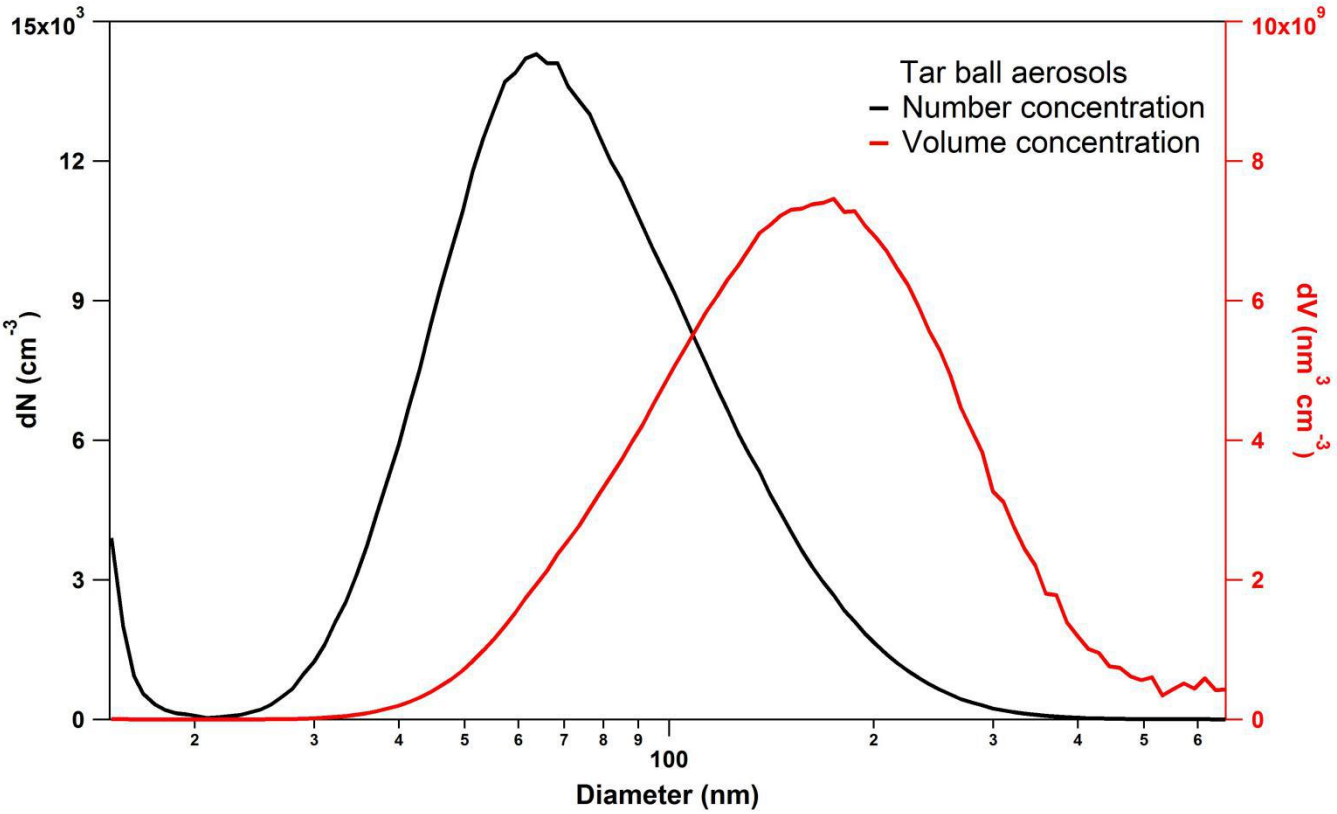

Figure S1. Size distribution of laboratory generated tar ball aerosols at downstream of the OFR.

2. Organic elemental ratios for fresh tar ball aerosols were derived from AMS measurement at W mode, and effective densities of tar ball aerosols were calculated from aerodynamic diameter divided by mobility diameter assuming tar ball with sphericity of 1.0

Table S1. Summary of fresh tar ball particles chemical elemental ratios and effective densities

BBOA	Mass spectra			Density (g cm^{-3})	Reference
	O:C	H:C	M/z>100 fraction		
Nonpolar	0.25±0.01	1.55±0.01	0.32	1.24±0.01	this work
Mixture (2:1 in vol.)	0.30±0.01	1.59±0.02	0.29	1.27±0.02	
Mixture (1:1 in vol.)	0.36±0.01	1.62±0.04	0.27	1.29±0.02	
Mixture (1:2 in vol.)	0.39±0.01	1.61±0.03	0.24	1.30±0.01	
Polar	0.44±0.02	1.64±0.03	0.15	1.33±0.02	
BBOA	0.3~0.4				Aiken et al., 2008
BBOA	0.29~0.33	1.51~1.58			Li et al., 2012
BBOA	0.18~0.26	1.4~1.5			He et al., 2010
BBOA	0.15~0.7	1.5~1.6	0.11~0.20	1.4	Zhou et al., 2017
BBOA				1.5	Sedlacek III et al., 2018
BBOA	0.33	1.90		1.18~1.19	Sumlin et al., 2017; 2018

3. Aerodynamic size distribution for tar ball particles measured by SP-LD-REMPI-ToF-MS

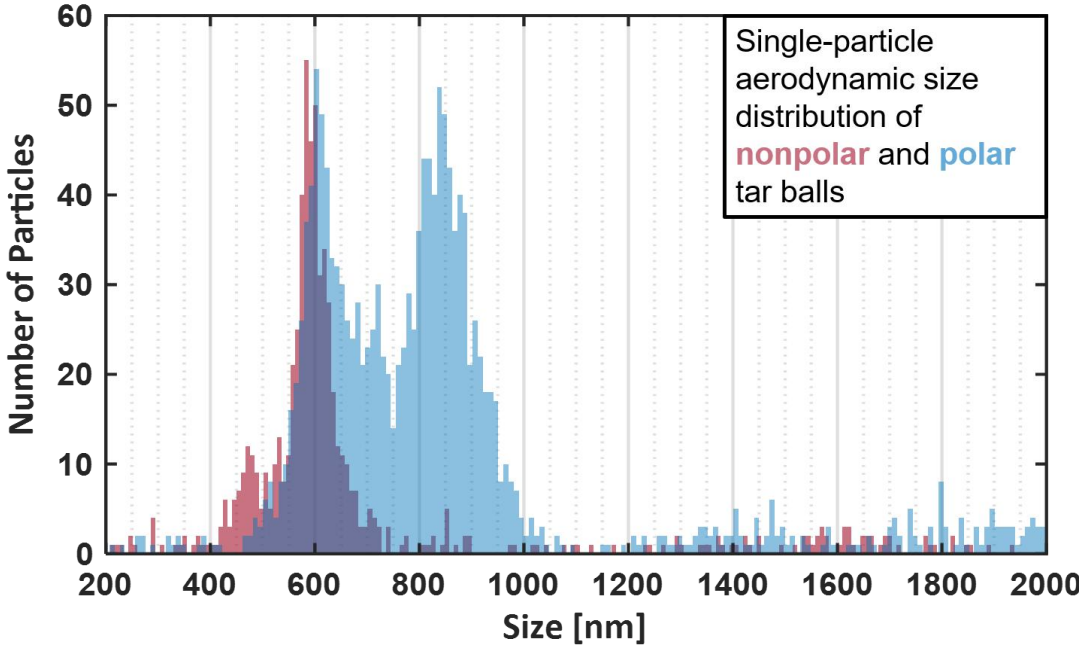

Figure S2. Particle aerodynamic size distributions for fresh nonpolar (red) and polar (blue) tar ball aerosols measured via laser velocimetry by the SP-LD-REMPI-ToF-MS instrument. The major mode peaks at about 550 nm for both particle classes while a second mode of larger particles occurs for polar tar balls and a second mode of smaller particles appears for nonpolar tar balls. Note that the detection efficiency drops rapidly below 250 nm due to the descending Mie scattering efficiency for particles much smaller than the wavelength (532 nm).

4. Exemplary Polyaromatic Compounds indicated by the REMPI PAH Spectra in this study (Table S2)

Table S2.Exemplary (poly)aromatic compounds indicated by the REMPI PAH Spectra in Figure 3

m/z	Name	Formula	Polar tar ball	Nonpolar tar ball	BBOA Reference
110	Catechol	$C_6H_6O_2$	√		Veres et al., 2010; Yee et al., 2013
115	PAHs fragments		√	√	Adler et al., 2011; Bruns et al., 2015
124	Guaiacol	$C_7H_8O_2$	√		Li et al., 2017; Yee et al., 2013; Hoffmann et al., 2007
128	Naphthalene	$C_{10}H_8$	√	√	Samburova et al., 2016; Passig et al., 2017; Bruns et al., 2015
138	4-Methylguajacol	$C_8H_{10}O_2$	√	√	Adler et al., 2011; Yee et al., 2013
152	Vanillin 4-Ethylguajacol	$C_8H_8O_3$ $C_9H_{12}O_2$	√	√	Li et al., 2014; Passig et al., 2017;Yee et al., 2013; Hoffmann et al., 2007
158	Methoxynaphthalene 1,4-Naphthalenedione Methylnaphthol	$C_{11}H_{10}O$ $C_{10}H_6O_2$ $C_{11}H_{10}O$	√		Santos et al., 2016; Yee et al., 2013; Hoffmann et al., 2007
165	PAHs fragments		√	√	Adler et al., 2011; Bruns et al., 2015
168	4-Methylsyringol Vanillic acid	$C_9H_{12}O_3$ $C_8H_8O_4$	√		Santos et al., 2016; Hoffmann et al., 2007; Bruns et al., 2015
178	Phenanthrene Conifery aldehyde	$C_{14}H_{10}$ $C_{10}H_{10}O_3$	√	√	Samburova et al., 2016; Bente et al., 2008, 2009; Passig et al., 2017
182	Syringaldehyde 4-Ethylsyringol	$C_9H_{10}O_4$ $C_{10}H_{14}O_3$	√		Santos et al., 2016; Yee et al., 2013; Hoffmann et al., 2007
189, 190, 191	Retene fragments		√	√	Bente et al., 2008, 2009; Mandalakis et al., 2005
192	Methylphenanthrene	$C_{15}H_{12}$	√	√	Samburova et al., 2016; Bente et al., 2008, 2009; Passig et al., 2017
202	Pyrene Fluoranthene	$C_{16}H_{10}$	√	√	Adler et al., 2011; Bente et al., 2008, 2009; Passig et al., 2017
203, 204, 205	Retene fragments		√	√	Passig et al., 2017; Mandalakis et al., 2005
206	Ethylphenanthrene	$C_{16}H_{14}$		√	Samburova et al., 2016
219, 220	Retene fragments		√	√	Bente et al., 2008, 2009; Passig et al., 2017
234	Retene	$C_{18}H_{18}$	√	√	Samburova et al., 2016; Bente et al., 2008, 2009; Passig et al., 2017

248	**Methyl. Retene**	**$C_{19}H_{20}$**		√	**Passig et al., 2017; Mandalakis et al., 2005**
250	**Ox. Retene**	**$C_{18}H_{18}O$**	√	√	**Samburova et al., 2016**

Note: only some major aromatic compounds were listed in the table

5. Morphology of tar ball aerosols (Figure S3)

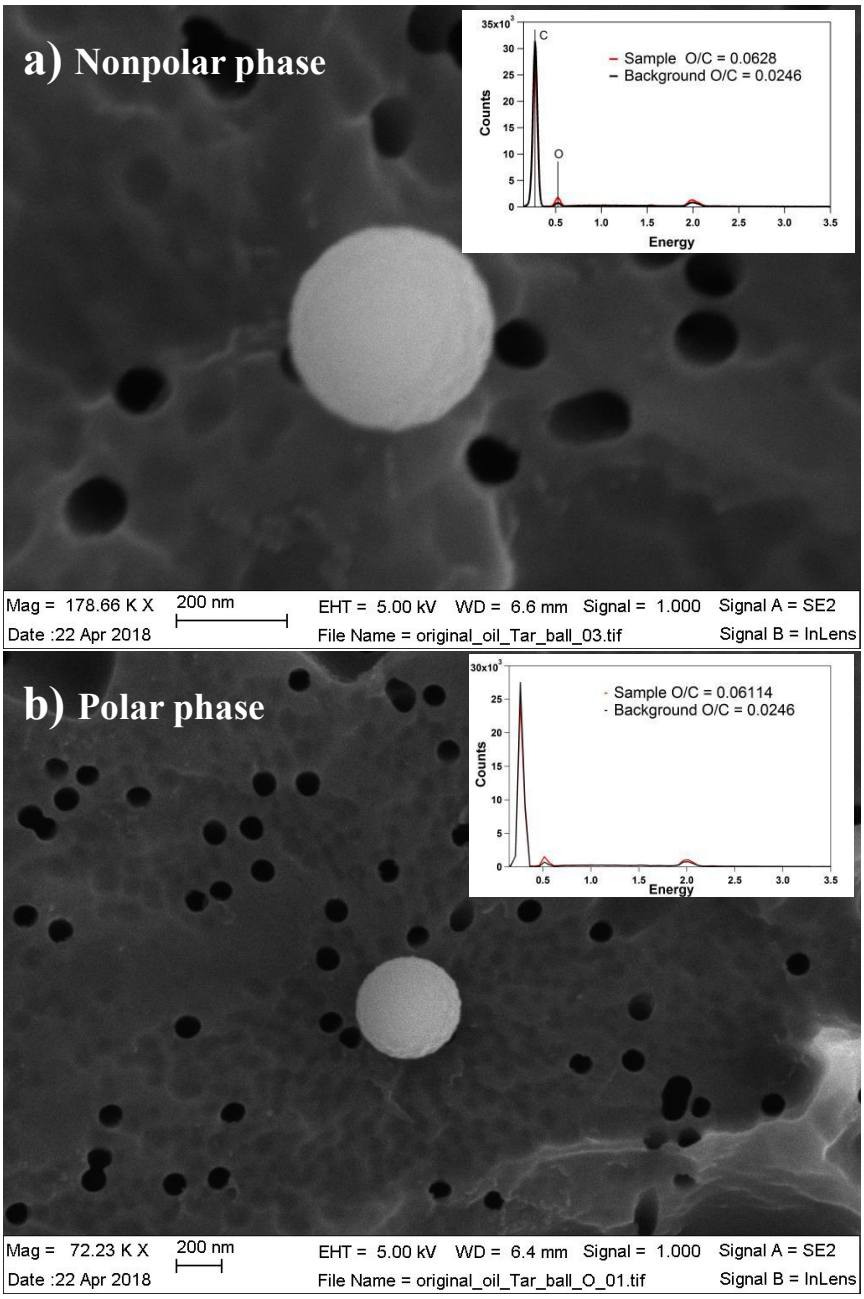

Figure S3. Morphology of fresh tar ball particles generated from polar and nonpolar phase tarry solutions. The particles are perfect spherical and amorphous in internal composition.

6. Refractive index for tar ball at mixture of 2:1 and 1:2 in volume of polar and nonpolar materials

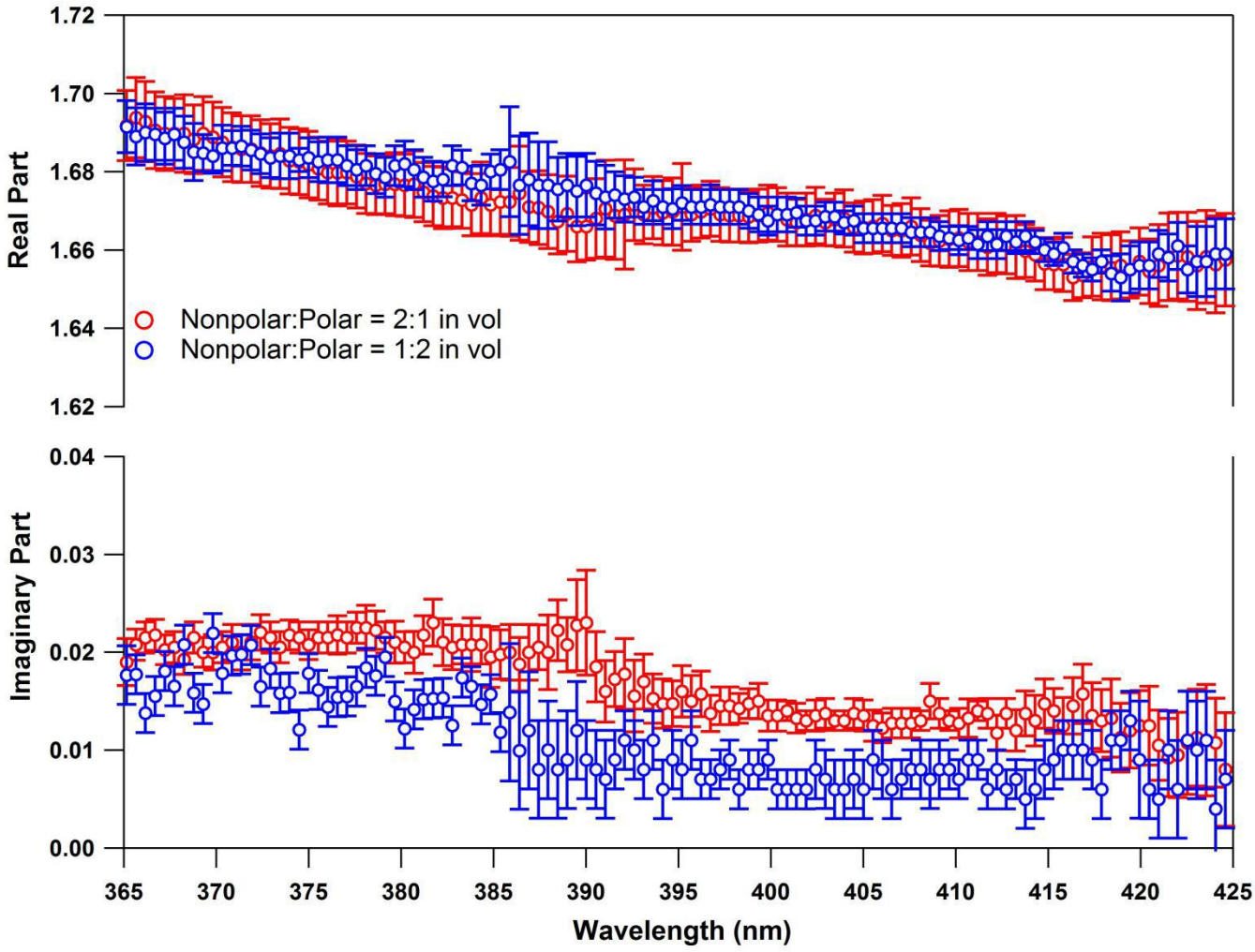

Figure S4. Wavelength-dependent refractive index (RI) for tar ball particles generated from polar and nonpolar phase solution mixtures

7. Example of absorption coefficients for some of the most absorbing PAHs identified in BBOA

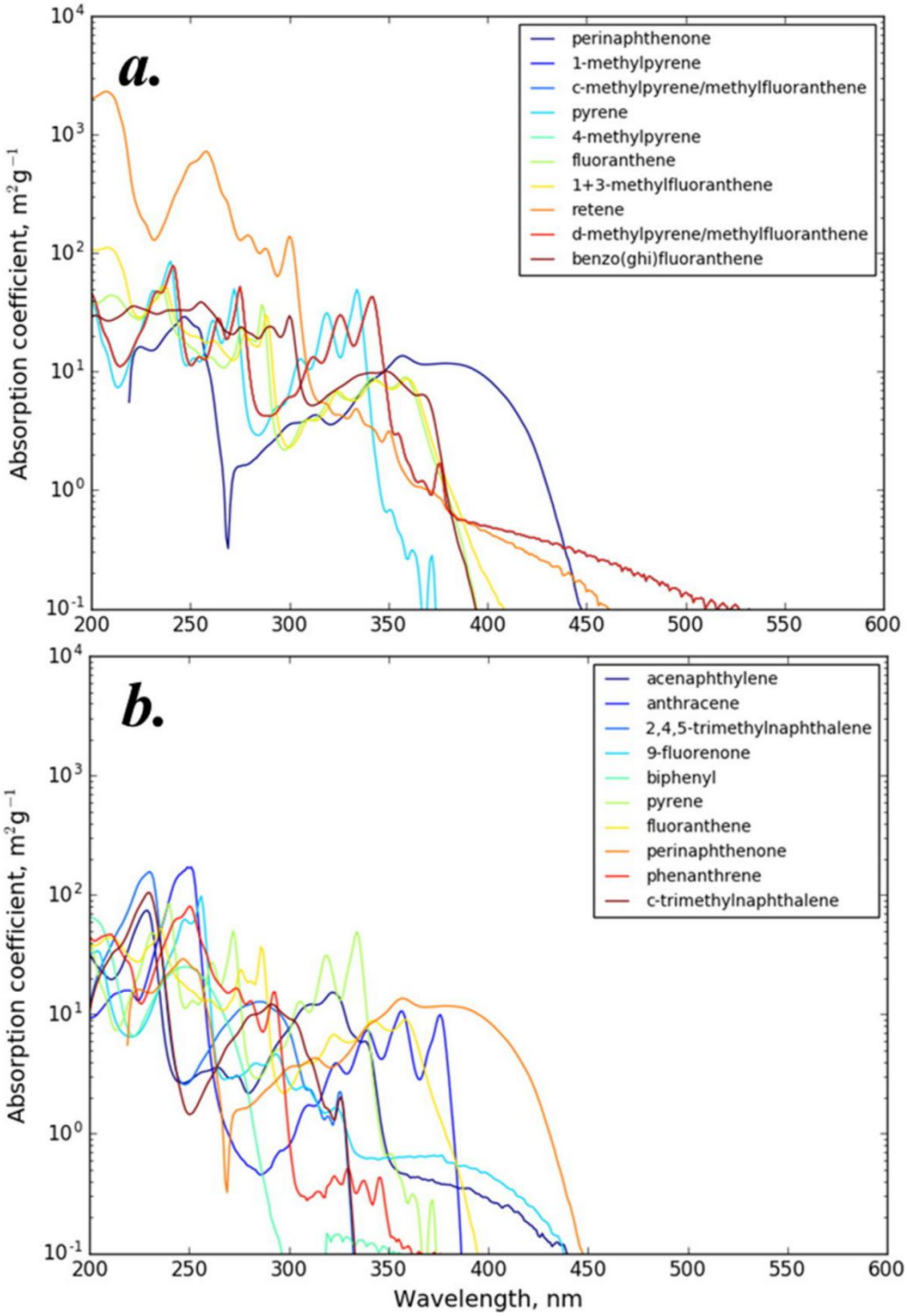

Figure S5. Absorption coefficients for some of the most absorbing PAHs identified in biomass burning emissions (Samburova et al., 2016).

8. Mass absorption cross sections (MAC) for fresh tar ball aerosols from 360 to 450 nm

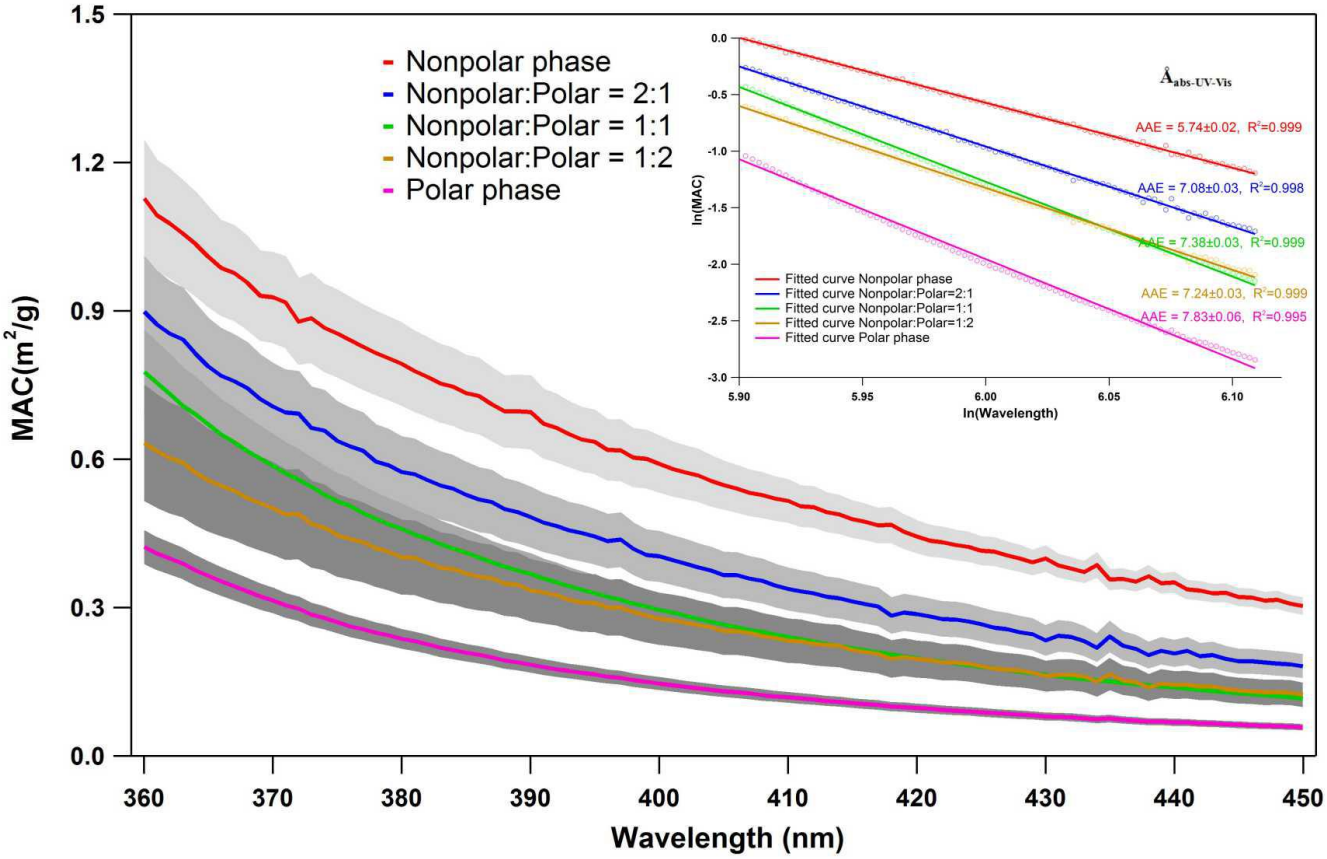

Figure S6. Mass absorption cross section (MAC) for methanol extracted fresh tar ball particles. Inset chart presents example of $Å_{abs\_UV\text{-}Vis}$ calculated from natural logarithm regression of MAC and wavelength.

9. Prediction of mixture tar ball optical properties based on different mixing rules

There are many mixing rules currently in use to predict optical properties of aerosol from matrix of various substances: 1) molar refraction and absorption (Jacobson, 2002; Tang, 1997); 2) a volume-weighted linear average of the refractive indices (d'Almeida et al., 1991); 3) the Maxwell-Garnet rule (Chýlek et al., 1984); and 4) the dynamic effective medium approximation (Jacobson, 2006). Due to the complexity of undefined chemical composition of tar ball particles, the Maxwell-Garnet and dynamic effective medium approximation are not feasible in this study, therefore, the simple molar fraction and volume-weighted mixing rules were discussed to fit the optical results.

The "linear mixing rule" simplifies mixing state and interaction between matrix, assumes that total real and imaginary refractive indices of the mixture are result of the indices of the components weighted by their their volume fractions:

$$\begin{aligned} n_{tot} &= \sum_n f_i n_i \\ k_{tot} &= \sum_n f_i k_i \end{aligned} \tag{1}$$

Where f_i, n_i, and k_i are the volume fraction, real part, and imaginary part of each component

The molar fraction mixing rule assumes that the total molar refraction of a mixture is given by the linear average of the molar refraction of each component weighted by their molar volumes, i.e.,

$$\begin{aligned} &\frac{\overline{M}}{\rho}\frac{n^2-1}{n^2+2} = \sum_n \chi_i \frac{M_i}{\rho_i}\frac{n_i^2-1}{n_i^2+2} \\ &\frac{\overline{M}}{\rho}k = \sum_n \chi_i \frac{M_i}{\rho_i}k_i \\ &\sum_n \chi_i = 1 \end{aligned} \tag{2}$$

Where x_i, M_i, and ρ_i are the molar fraction, molecular weight, and material density.

Refractive indices for tar ball generated from polar and nonpolar fraction mixture at solution mixing ratios of 1:2,1:1, and 2:1 will be calculated from RI of polar and nonpolar optical results based on above two rules. The exact volume and molar fraction for bulk polar and nonpolar part in particles can be estimated from particle density and chemical elemental ratios:

$$\begin{aligned} &\rho_{tot} = f_1\rho_1 + f_2\rho_2 \\ &f_1 + f_2 = 1 \end{aligned} \tag{3}$$

$$\begin{aligned} &R_{\overline{O/C}} = \chi_1 R_{\overline{O/C}_1} + \chi_2 R_{\overline{O/C}_2} \\ &\chi_1 + \chi_2 = 1 \end{aligned} \tag{4}$$

Where $R_{O/C}$ is oxygen to carbon ratio from AMS measurement of tar ball particles, and calculated particulate volume and molar fraction are given below:

Table S3. Particulate molar and volume fractions of bulk polar and nonpolar tar

Polar:Nonpolar prepared solution ratio	O/C molar ratio	O/C retrieved molar mixing ratio	Density (g cm^{-3})	density retrieved volume mixing ratio
1:0	0.44	1:0	1.329±0.021	1:0
2:1	0.39	2.8:1	1.298±0.022	1.8:1
1:1	0.36	1.375:1	1.285±0.019	0.98:1
1:2	0.3	1:2.8	1.274±0.013	1:1.72
0:1	0.25	0:1	1.242±0.005	0:1

Molecular weight for polar and nonpolar fractions were simplified as $M_{\text{bulk-polar}}$ and $M_{\text{bulk-nonpolar}}$, and mixture tar ball particles follow the function below:

$$\frac{\overline{M}}{\overline{\rho}} = \frac{x_1 M_{bulk-polar}}{\rho_1} + \frac{x_2 M_{bulk-nonpolar}}{\rho_2}$$
$$\overline{M} = x_1 M_{bulk-polar} + x_2 M_{bulk-nonpolar} \quad (5)$$

And it was calculated as $M_{\text{bulk-nonpolar}} \approx 1.3 M_{\text{bulk-polar}}$

For convenience and clarity, wavelength-dependent RI for tar ball were exponential or power-law fitted, the results were showed in Figure S6 and corresponded parameters were summarized in Table S4:

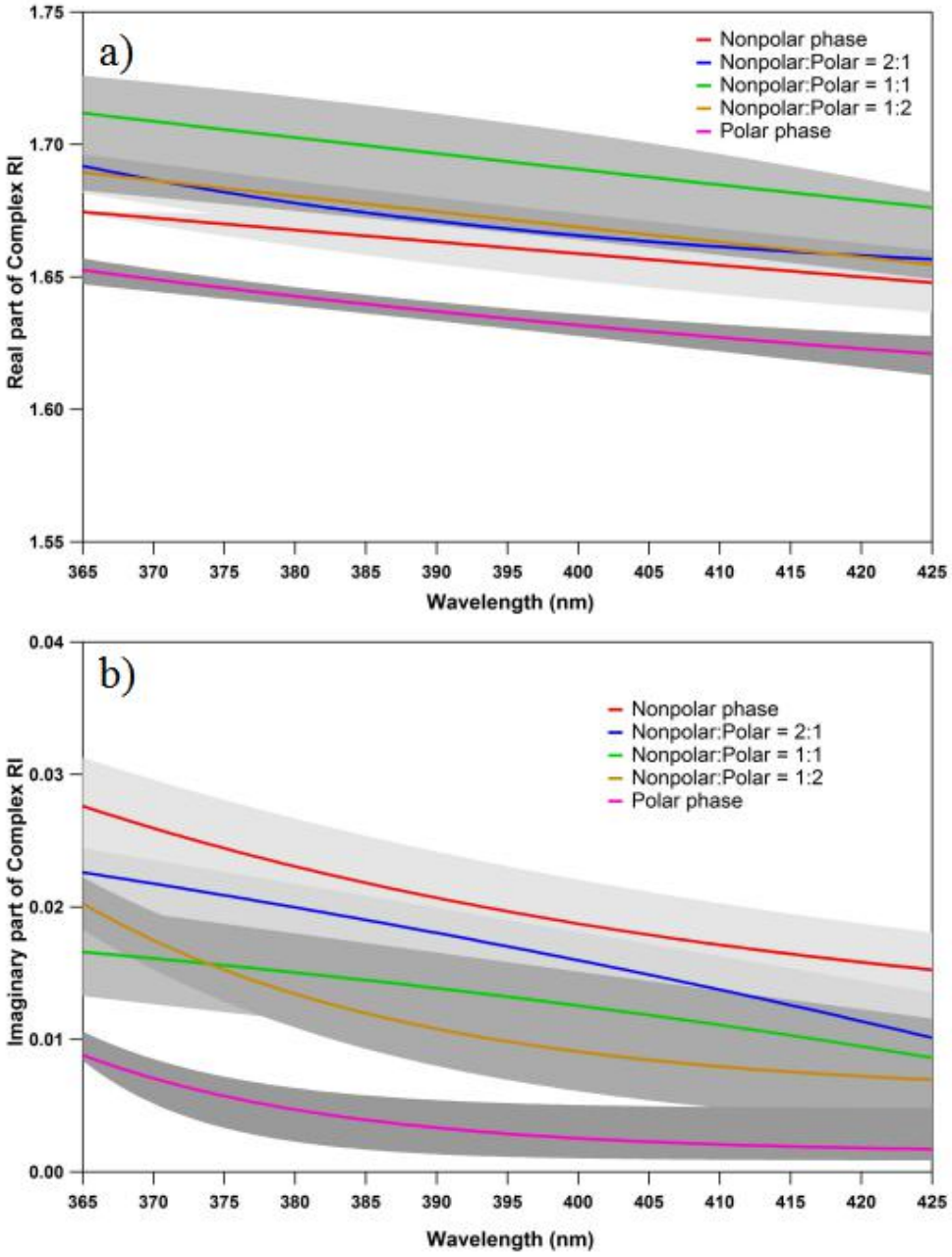

131

132 **Figure S7.** Regressed RI for tar ball particles of various mixing ratios: a) real part, and b) imaginary part

133

Table S4. Parameterization of the Wavelength-Dependent (365 to 425 nm) Effective Complex RI of tar ball particles

Tar ball		Real			Imaginary		
		Co	C1	C2	Co	C1	C2
Nonpolar phase	min	1.604	7.148	-1.27E-02	0.164	-8.89E-02	1.27E-03
	average	1.033	0.831	-7.08E-04	0.010	2.37E+01	-1.97E-02
	max	1.677	-1.95E-09	3.80E-02	0.010	8.75E+00	-1.65E-02
Nonpolar:polar 2:1	min	1.627	22.067	-1.65E-02	0.028	-1.05E-05	1.80E-02
	average	1.646	321.800	-2.43E-02	0.046	-1.81E-03	7.06E-03
	max	1.658	2819.637	-3.04E-02	0.330	-2.47E-01	5.86E-04
Nonpolar:polar 1:1	min	1.657	55.140	-1.98E-02	-0.291	3.52E-01	-4.01E-04
	average	1.324	0.697	-1.61E-03	0.023	-5.69E-16	5.10E+00
	max	1.754	-5.09E-18	6.145	-0.220	3.00E-01	-6.09E-04
Nonpolar:polar 1:2	min	1.832	-0.044	3.35E-03	0.002	6.88E+04	-4.19E-02
	average	1.306	0.683	-1.58E-03	0.006	8.43E+04	-4.27E-02
	max	1.550	0.826	-4.75E-03	0.009	1.56E+40	-1.64E+01
Polar phase	min	1.921	-0.133	1.97E-03	0.016	-5.83E-19	6.33E+00
	average	1.585	3.174	-1.06E-02	0.001	3.02E+06	-5.43E-02
	max	1.615	53.051	-1.95E-02	0.005	5.43E+11	-8.81E-02

Note: Non-shaded cells were fitted with an exponent; $n\&k(\lambda)=C_0+C_1\times e^{(C2\times\lambda)}$. Shaded cells were fitted with a power law; $n\&k(\lambda)=C_0+ C_1^{\lambda\times C2}$

The calculated RI following "volume linear mixing rules" for tar ball were presented in Figure S8 and compared with experimental data in Figure S9.

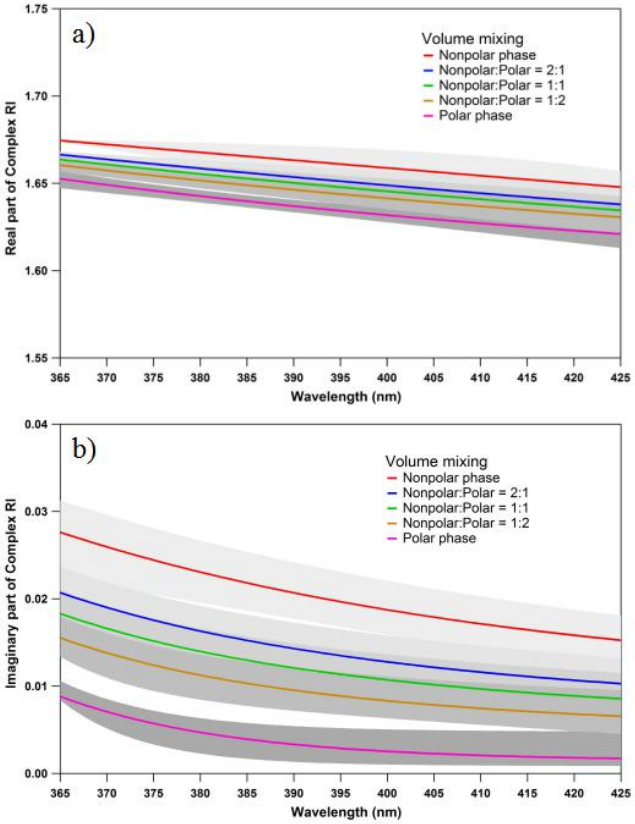

139

140 **Figure S8**. Estimated RI for tar ball particles of various mixing ratios based on volume linear mixing rule: a) real part, and b)
141 imaginary part

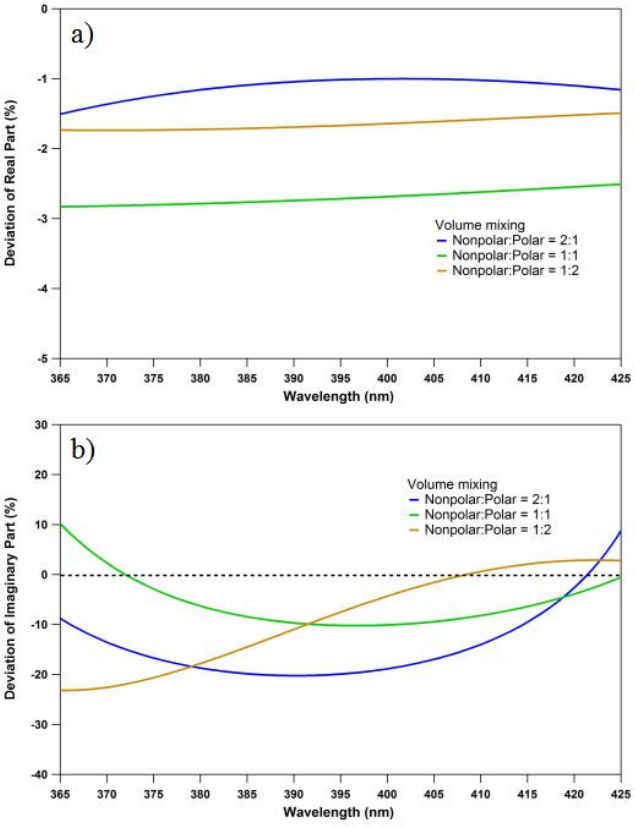

142

143 **Figure S9**. Deviation between experimental RI and predicted RI from volume linear mixing rule: a) real part, and b) imaginary
144 part

145

The calculated RI following "molar fraction mixing rules" for tar ball were presented in Figure S10 and compared with experimental data in Figure S11.

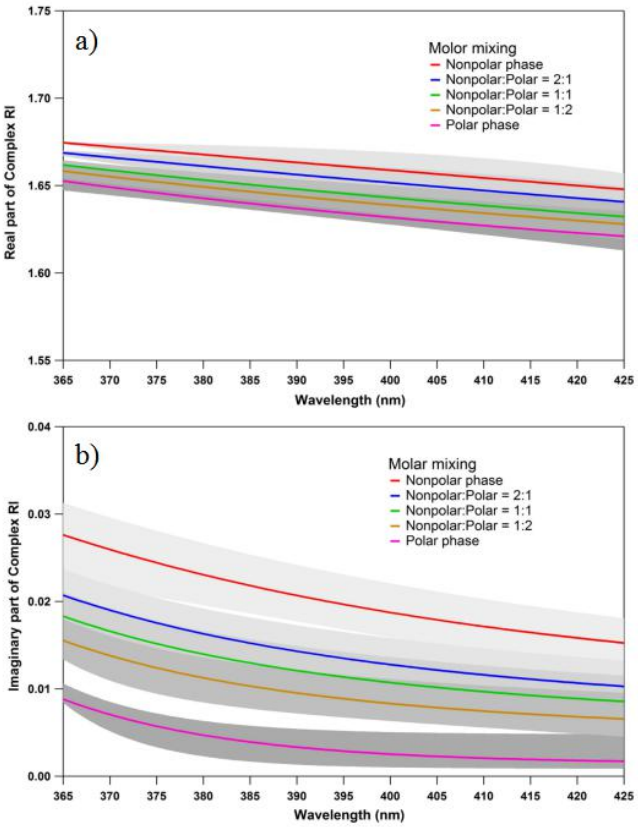

Figure S10. Estimated RI for tar ball particles of various mixing ratios based on molar fraction mixing rule: a) real part, and b) imaginary part

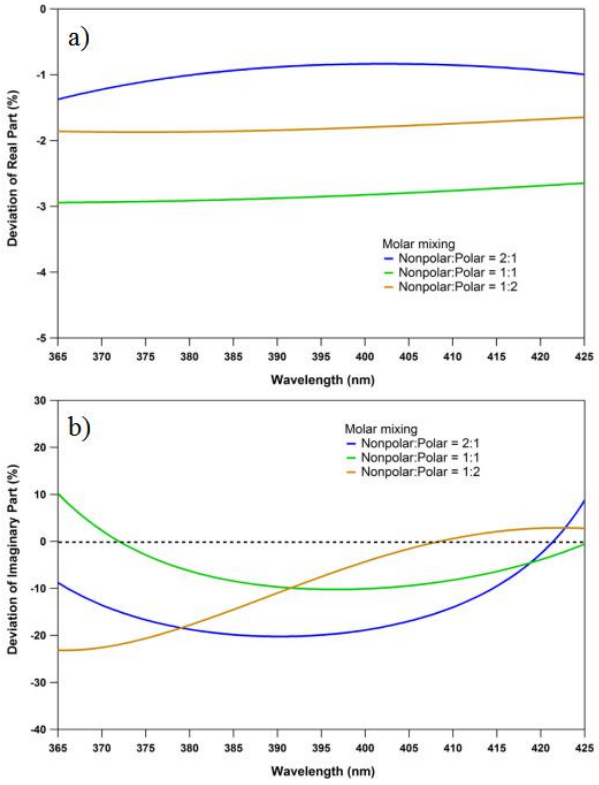

Figure S11. Deviation between experimental RI and predicted RI from molar fraction mixing rule: a) real part, and b) imaginary part

10. Summary of optical parameters for tar ball aerosol upon NOx-dependent photochemical aging

Table S5. Summary of RI and Ångström exponent changes for tar ball particles upon photochemical oxidation (mean ± standard deviation)

Tar ball	Complex Refractive index			SSA (average)	$Å_{abs}$	$Å_{abs\_UVVIS}$	$Å_{ext}$
	Average	375nm	405nm				
Fresh	(1.661±0.008)+(0.020±0.004)i	(1.671±0.003)+(0.025±0.003)i	(1.659±0.011)+(0.017±0.002)i	0.89 ± 0.01	5.87 ± 0.37	6.74	3.81 ± 0.18
O_0.7	(1.641±0.010)+(0.014±0.006)i	(1.652±0.001)+(0.021±0.001)i	(1.635±0.001)+(0.010±0.002)i	0.92 ± 0.02	9.33 ± 3.38	6.11	4.21 ± 0.07
O_1.7	(1.639±0.011)+(0.008±0.005)i	(1.651±0.002)+(0.015±0.004)i	(1.631±0.002)+(0.005±0.003)i	0.96 ± 0.03	10.96 ± 3.23	6.46	4.33 ± 0.04
O_3.9	(1.632±0.010)+(0.007±0.004)i	(1.643±0.001)+(0.011±0.002)i	(1.628±0.002)+(0.004±0.001)i	0.96 ± 0.02	10.63 ± 3.17	6.31	4.11 ± 0.09
O_6.7	(1.624±0.007)+(0.007±0.003)i	(1.630±0.003)+(0.009±0.003)i	(1.623±0.002)+(0.004±0.003)i	0.96 ± 0.02	9.89 ± 2.59	6.02	3.74 ± 0.06
N_0.5	(1.635±0.011)+(0.015±0.004)i	(1.646±0.001)+(0.018±0.001)i	(1.629±0.001)+(0.012±0.002)i	0.91 ± 0.01	6.92 ± 1.35	6.41	4.01 ± 0.07
N_2.0	(1.648±0.008)+(0.019±0.004)i	(1.653±0.002)+(0.025±0.003)i	(1.645±0.002)+(0.016±0.001)i	0.89 ± 0.01	5.60 ± 0.69	6.35	3.76 ± 0.10

11. Mass absorption cross sections (MAC) for NOx-free photochemical aged tar ball aerosols from 360 to 450 nm

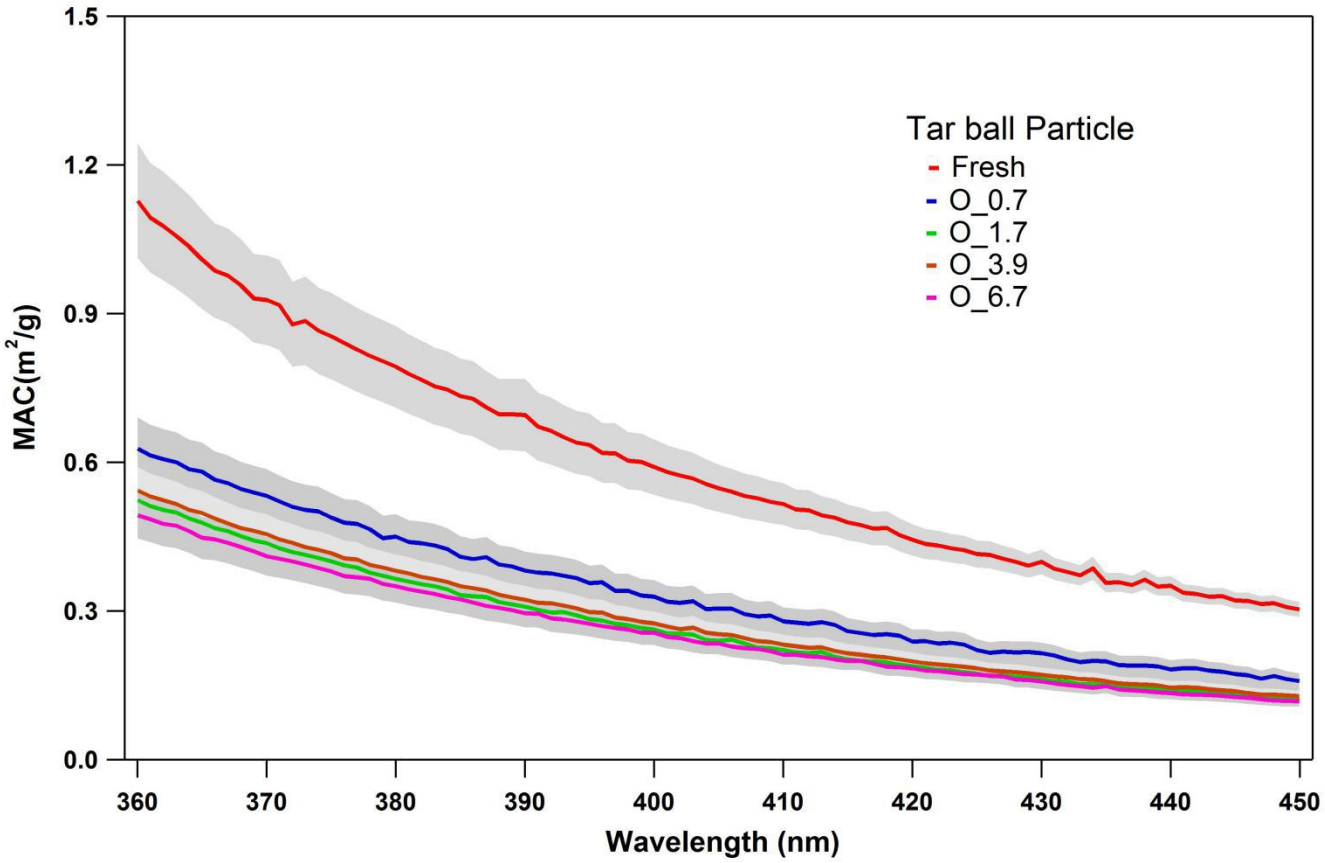

Figure S12. Diminishing in tar ball mass absorption cross section (MAC) upon daytime NOx-free photochemical oxidation

12. Optical and chemical changes for tar ball aerosols due to photolysis from UV light irradiation in the OFR

Studies have reported that BrC formation and SOA decomposition due to directly UV/near UV-short visible light irradiation of various precursors in both liquid and air (Bateman et al., 2011; Malecha and Nizkorodov, 2016; Wong et al., 2017). During photochemical aging through the OFR at residence time of 144s, tar ball particles were also exposed to high photon flux at 254 nm. We performed several experiments to estimate the influence of UV illumination on tar ball evolution. Irradiation tests of P1 and P2 repeated the same aging process of O_1.7 and O_3.9 without external O_3, and P3 was conducted at a full power of the UV lamps in the OFR. We observed slight chemical composition changes in the tar ball aerosols due to photolysis, as the O/C ratio continuously increased while H/C decreased with extension of irradiation (Table S6 and Figure S13). The O/C ratio increased by 0.04 for maximal irradiation exposure, which was much smaller than that from photochemical oxidation. This indicates that OH-initiated oxidation rather than photolysis reactions play a more dominate role in tar ball aging.

The decrease of the H/C ratio due to photolysis exhibited a distinct different chemical pathway than by OH photooxidation. According to the mass spectra analysis, particularly for the P3 experiment shown in Figure S14, the fractions of signals attributed to $C_xH_y^+$ and $C_xH_yO_z^+$ fragments decreased, and as a consequence, the contribution of the $C_xH_yO^+$ fractions increased in photolyzed tar ball aerosols. Comparing to the fresh tar ball mass spectra, alkyl/alkenyl chains, carboxylic acids/peroxides (CO_2^+, CHO_2^+), and carbonyl/aldehyde groups (CO^+, CHO^+, $C_2H_3O^+$) fragments depleted due to irradiation by UV light. Furthermore, increase of the *f*44/*f*43 ratio with photolysis shown in Figure S14, indicates decay of CO_2^+ to a less extent compared to the loss of $C_2H_3O^+$. Photolysis occurs in the condensed phase as particles containing photolabile compounds that efficiently absorb light at actinc wavelengths. Oxygenated species such as carbonyls, carboxylic acids, and peroxides are more vulnerable to photolysis, especially in the UV. With cleavage of the oxygenated functional groups, molecules become more volatile and may desorb to the gas phase (Henry and Donahue, 2012). Considerable amount of VOCs productions, including small molecular acids, ketones, aldehydes (e.g., acetic acid, formic acid, acetaldehyde, acetone, etc.), and hydrocarbon species (e.g., methane, ethene, propane, etc.), were detected from photo-degradation of various SOA (Malecha and Nizkorodov, 2016; Mang et al., 2008), and photocleavage of carbonyls has been emphasized in photolysis of SOA. Bateman et al. (2011) reported that exposure to UV irradiation increased the O/C ratio of dissolved ambient SOA, and they attributed the chemical changes to photodissociation of molecules containing carbonyl groups and net production of carboxylic acids that overweigh their decomposition in pH modified solution. Detailed mechanisms were proposed such as n-π^* Norrish type-I and -II splitting of carbonyls and n-σ^* photolysis of peroxides to form production of carboxylic acids in the presence of dissolved oxygen (Norrish, 1934; Pitts et al., 1964).

In the current experiments, photolysis occurred in particle phase which can be different from photolysis in liquid phase. First, the photolysis of particles should be less efficient as quenching is more likely and fragment caging can prevent rapid recombination. Second, photolysis products (volatile molecules and radicals) can more easily transfer to the gas phase rather than accumulate in the solution and be involved in further reactions. Epstein et al. (2014) isolated photolysis influence on α-pinene SOA. They reported suppression of SOA mass loading and marked decomposition of particle-bound organic peroxides from UV light illumination. The fraction of $C_xH_y^+$ fragments slightly decreased while the oxygenated fragments increased upon irradiation. Wong et al. (2014) highlighted RH-dependent photolysis as a sink for SOA in the atmosphere, in particular, photolysis results in more oxidized SOA due to kinetic preference for degradation of less oxidized components, and they attributed the slower decay of *f*44 (CO_2^+) to photodissociation of peroxides and the formation of carboxylic acids in SOA upon UV irradiation.

The optical properties of SOA can change upon photolysis of photolabile carbonyl/carboxylic organics, peroxides, and other chromophores. Liu et al. (2016) investigated the influences of various environmental factors on light absorption of aromatic SOA from ozonolysis in the presence of NO_x. They suggested that photolysis, rather than hydrolysis, bleached SOA absorption due to degradation of nitrogen-containing chromophores. This conclusion was also confirmed by similar studies by Lee et al. (2014) and Aiona et al. (2018). In our study, the changes in the optical properties as a function of O/C ratio for tar balls upon photolysis are

shown in Figure S15. The relevant parameters are summarized in Table S7, MAC changes for tar ball upon photolysis are presented in Figure S16. RI of both real and imaginary parts weakly diminished during irradiation, and the average RI at 375 nm decreased by 0.012+0.006i for maximum photolyzed tar ball, corresponded MAC at 375 nm decreased by ~31.3%.

Table S6. Summary of mass spectra characters and effective density changes for tar ball particles upon photolysis from UV light irradiation (mean ± standard deviation)

Tar ball	O:C	H:C	N:C	m/z>100 fraction	density
Fresh	0.25±0.01	1.55±0.01	0.012±0.002	0.32	1.24±0.01
P1	0.26±0.01	1.53±0.01	0.013±0.003	0.33	1.24±0.01
P2	0.27±0.01	1.51±0.01	0.011±0.001	0.32	1.24±0.01
P3	0.29±0.01	1.49±0.01	0.012±0.002	0.33	1.24±0.01

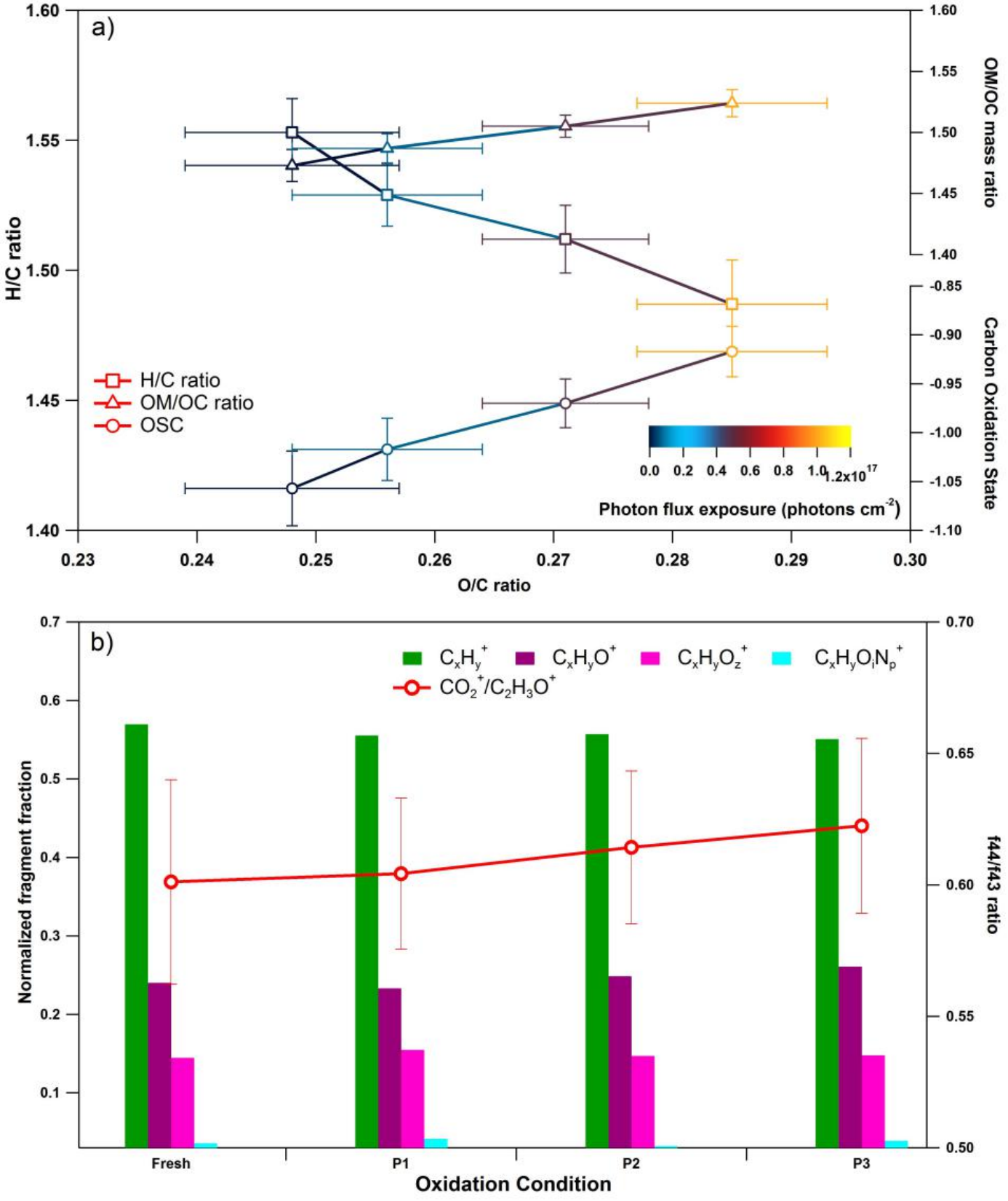

Figure S13. Dynamic changes for chemical characteristics of tar ball particle upon UV light irradiation: a) OM/OC, H/C ratio, and average carbon oxidation state ($\overline{OSc}$) changes as a function of O/C ratio; b) mass spectra evolution with photolysis extension in term of $C_xH_y^+$, $C_xH_yO^+$, $C_xH_yO_z^+$, and $C_xH_yO_iN_p^+$ fragment groups

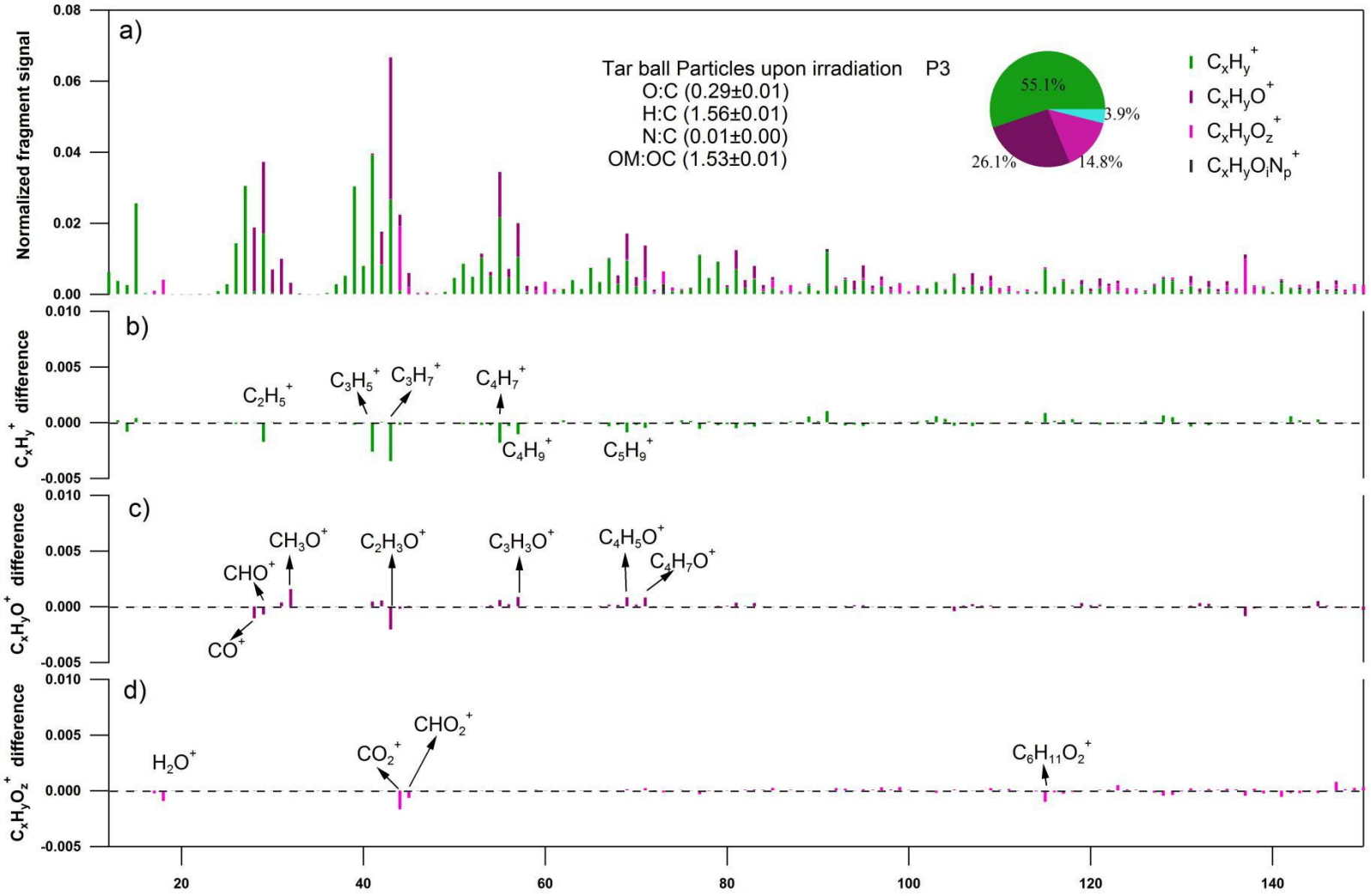

Figure S14. High-resolution mass spectra changes for nonpolar tar ball particles after maximum photolysis in P3 test, four ion groups were grouped for clarity as: $C_xH_y^+$, $C_xH_yO^+$, $C_xH_yO_z^+$ (z>1), $C_xH_yO_iN_p^+$(i≧0,p≧1). Ions O^+, OH^+, and H_2O^+ were included in the $C_xH_yO_z^+$ group. Mass fraction of the four fragment groups was pie-chart presented. a) normalized mass spectra of aged tar ball particles, b)~d) changes of $C_xH_y^+$, $C_xH_yO^+$, $C_xH_yO_z^+$, and $C_xH_yO_iN_p^+$ comparing with fresh tar ball normalized mass spectra

Table S7. Summary of RI and Ångström exponent changes for tar ball particles upon photolysis (mean ± standard deviation)

Tar ball	Complex Refractive index			SSA (average)	$Å_{abs}$	$Å_{abs\_UVVIS}$	$Å_{ext}$
	Average	375nm	405nm				
Fresh	(1.661±0.008)+(0.020±0.004)i	(1.671±0.003)+(0.025±0.003)i	(1.659±0.011)+(0.017±0.002)i	0.89 ± 0.01	5.87 ± 0.37	6.74	3.81 ± 0.18
P1	(1.658±0.010)+(0.022±0.006)i	(1.668±0.001)+(0.027±0.001)i	(1.653±0.002)+(0.018±0.001)i	0.88 ± 0.02	6.92 ± 0.60	6.59	3.94 ± 0.03
P2	(1.649±0.008)+(0.018±0.004)i	(1.656±0.002)+(0.023±0.002)i	(1.647±0.002)+(0.014±0.003)i	0.90 ± 0.02	6.99 ± 1.22	6.50	3.79 ± 0.05
P3	(1.649±0.010)+(0.015±0.004)i	(1.659±0.005)+(0.019±0.004)i	(1.644±0.004)+(0.013±0.003)i	0.92 ± 0.01	7.42 ± 0.53	6.56	4.01 ± 0.01

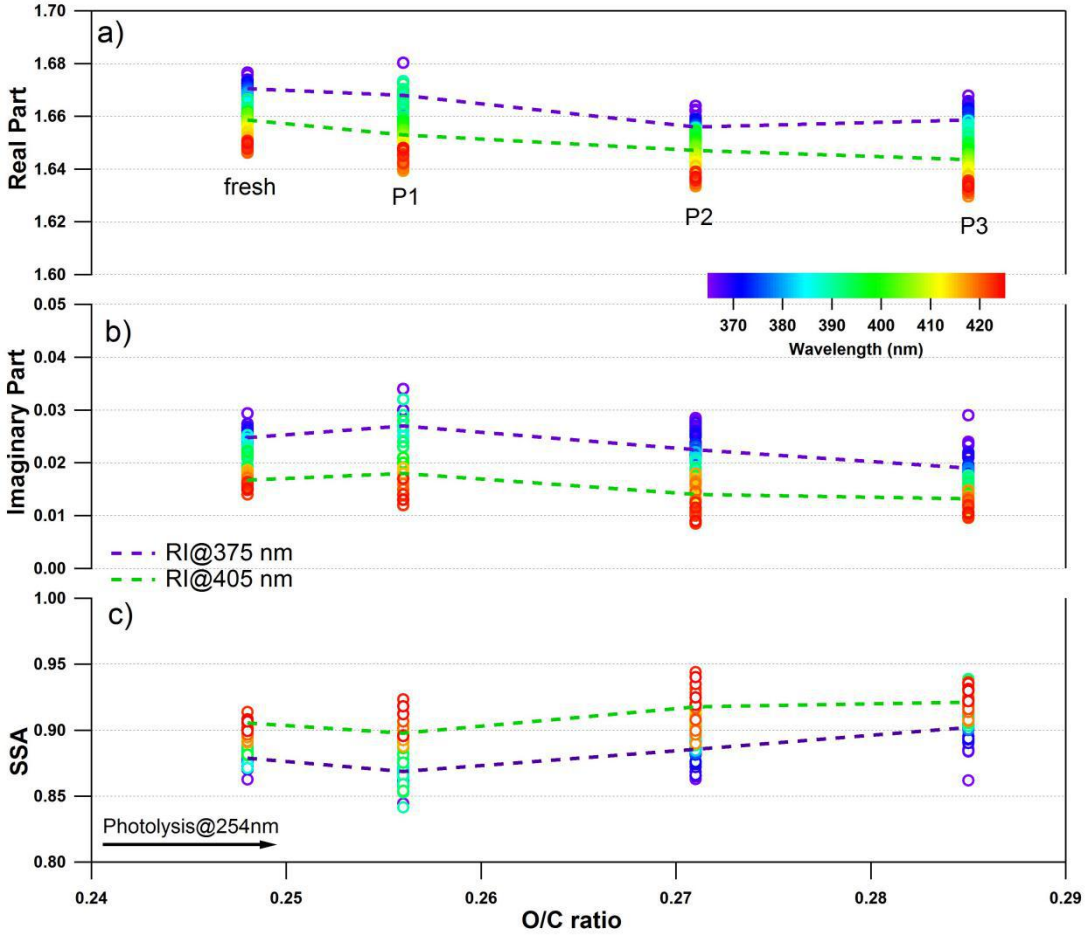

Figure S15. Changes in the retrieved spectral-dependent complex RI and SSA as a function of O/C ratio for tar ball particles upon 254 nm illumination: a) real part, b) imaginary part, and c) SSA calculated for 150 nm particles. The color scale shows the span in the RI for the wavelengths measured from 365 to 425 nm. For clarity, error bars for O/C ratio (±0.01), RI (±0.008 for real part, and ±0.003 for imaginary part on average) and SSA (±0.006) are not shown. The two dashed lines trace RI and SSA at 375nm (purple) and 405nm (green). P1~P3 represent photolysis studies with low to maximal photon flux exposures.

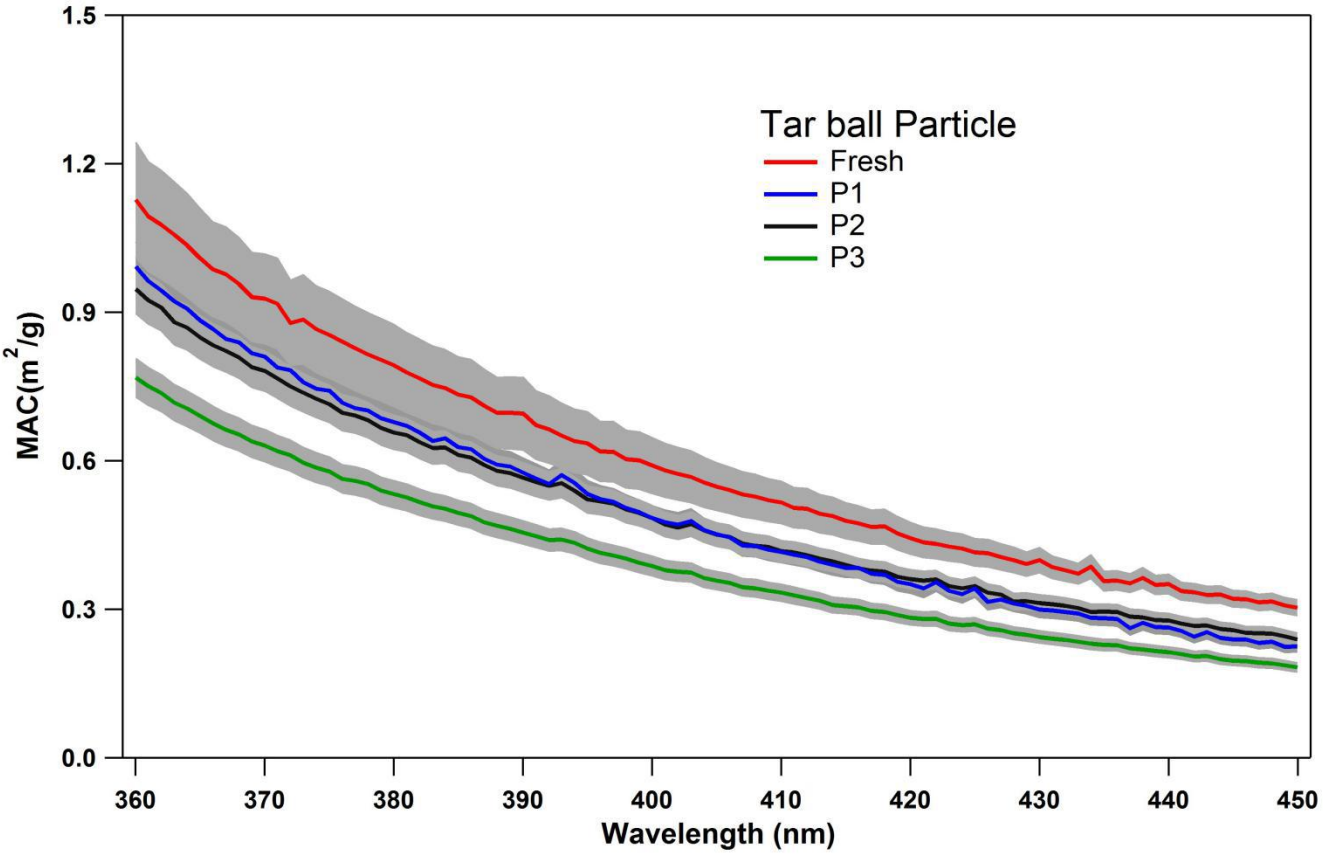

Figure S16. Changes of tar ball mass absorption cross section (MAC) as a function of wavelength upon UV photolysis

13. Optical and chemical changes of tar ball aerosols due to O_3 oxidation

Prior to photochemical aging experiments, blank test of tar ball oxidation via O_3 under dark was conducted in the OFR. Initial environmental conditions (e.g., O_3 and tar balls concentrations, relative humidity, residence time, etc) were maintained the same with following daytime evolution simulations, while UV lamps were not turned on. Dynamic optical and chemical changes for tar balls were characterized and presented in Figure S17 and S18. We did not observe significant refractive index changes for tar balls after 28.6 ppm O_3 oxidation, taking ambient O_3 concentration of 50 ppb, equivalent atmospheric O_3 exposure for tar balls through the OFR was about one day. RIs of fresh tar ball are (1.671±0.003)+(0.025±0.003)i and (1.659±0.011)+(0.017±0.002)i at 375 and 405 nm, respectively. After O_3 oxidation, RIs became (1.677±0.012)+(0.023±0.003)i and (1.668±0.011)+(0.013±0.004)i at at 375 and 405 nm, respectively. In Figure S18, O_3 oxidation weakly increased O/C and OM/OC ratios of tar balls, O/C ratio increased by 0.02 from initial 0.25, and OM/OC increased from 1.47 to 1.50, while H/C ratio remained during O_3 oxidation of tar ball particles. It was found $C_xH_y^+$ fractions slight decreased in compensation of more $C_xH_yO^+$ and $C_xH_yO_z^+$ fragments formation, indicating oxygenated moieties produced.

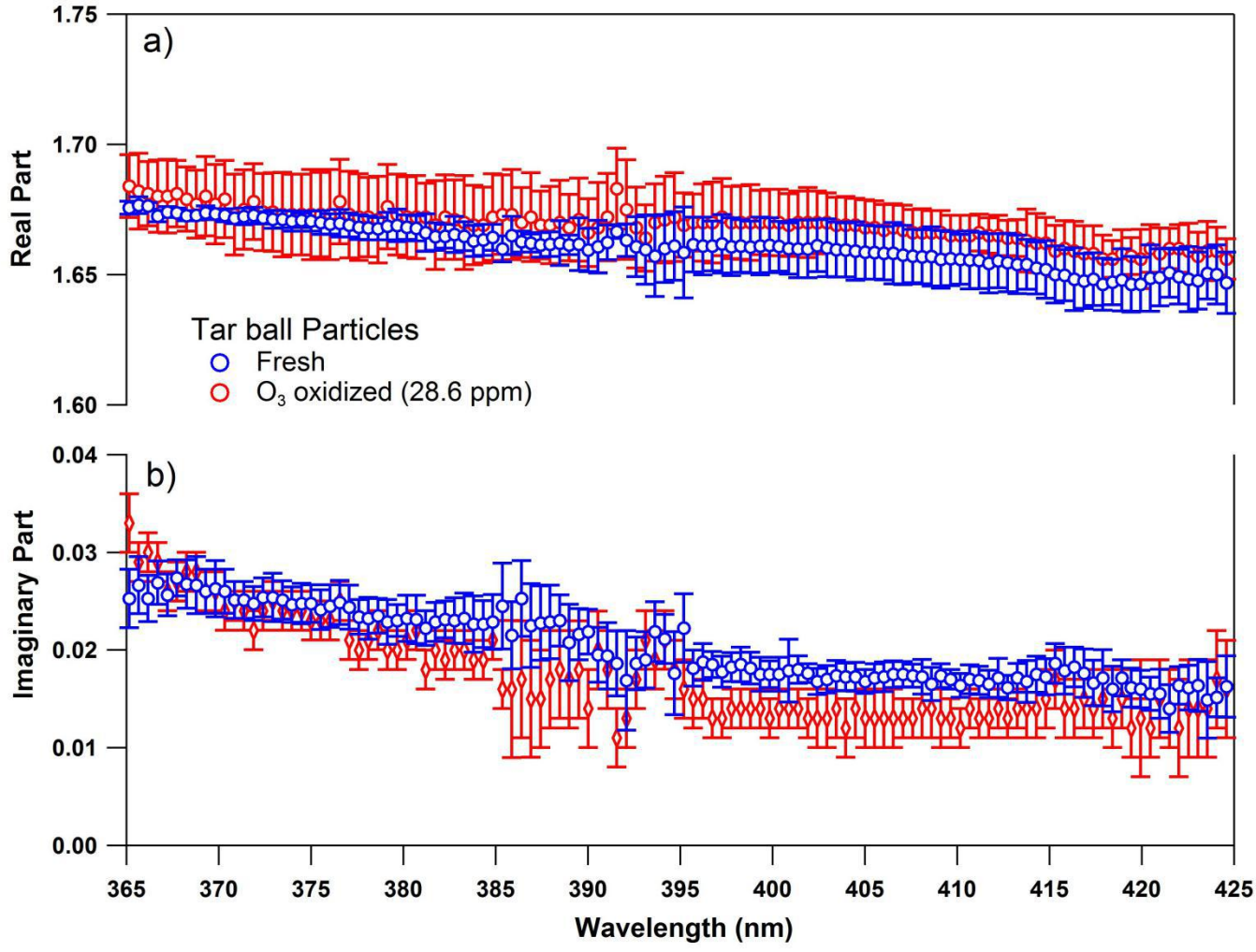

Figure S17. Refractive index as a function of wavelength for fresh and O3 oxidized tar balls, a) real part, b) imaginary part

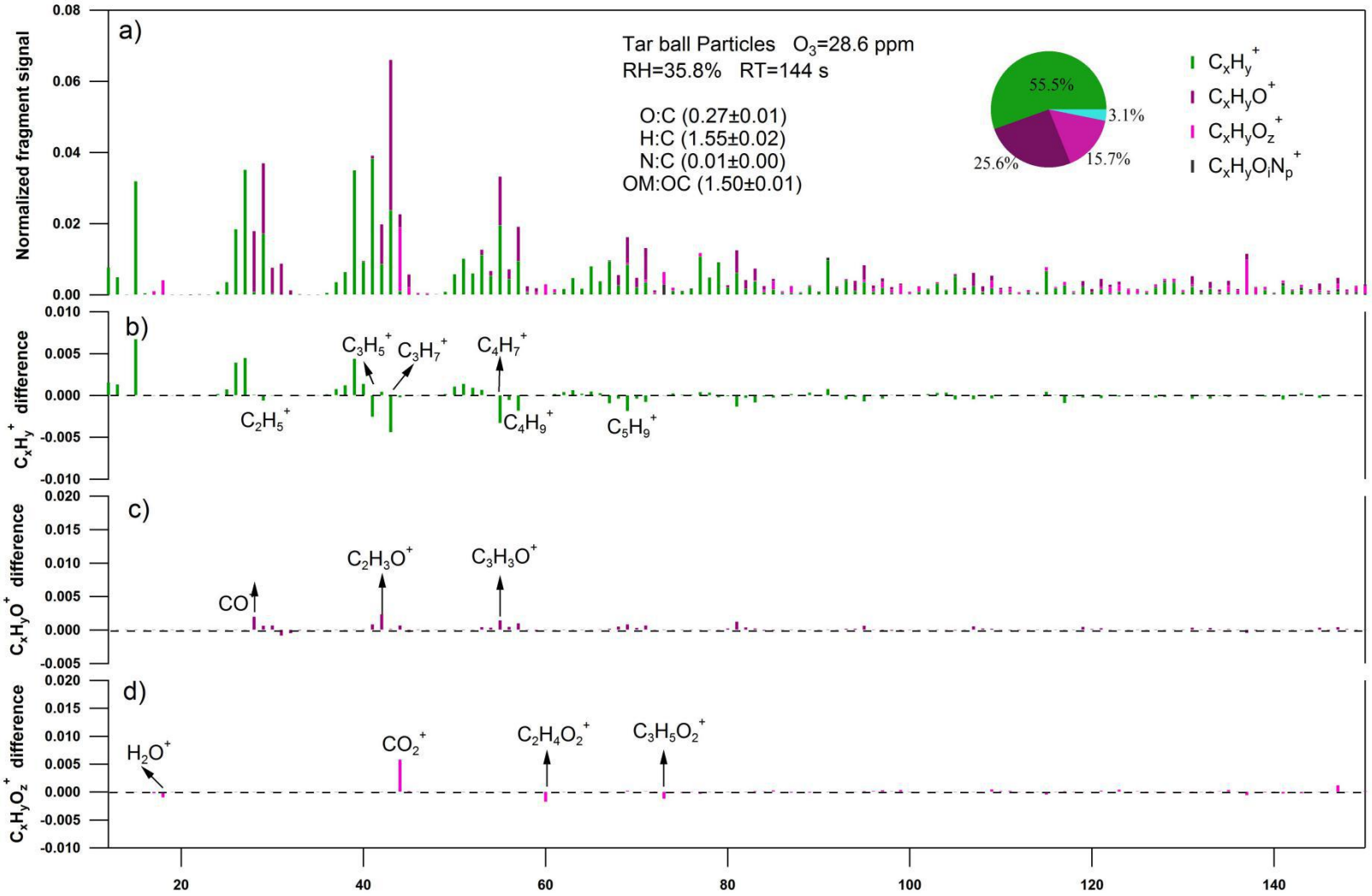

Figure S18. High-resolution mass spectral changes for nonpolar tar ball particles oxidized via O_3. Four ion groups were grouped for clarity: $C_xH_y^+$, $C_xH_yO^+$, $C_xH_yO_z^+$ (z>1), $C_xH_yO_iN_p^+$(i≧0,p≧1). Ions O^+, OH^+, and H_2O^+ were included in the $C_xH_yO_z^+$ group. Mass fraction of the four fragment groups was pie-chart presented. a) normalized mass spectra of O_3 oxidized tar ball particles, b)~d) changes of $C_xH_y^+$, $C_xH_yO^+$, $C_xH_yO_z^+$, and $C_xH_yO_iN_p^+$ comparing with fresh tar ball normalized mass spectra

14. Mass spectra characters and effective density changes for tar ball particles upon photochemical oxidation

Table S8. Summary of mass spectra characters and effective density changes for tar ball particles upon photochemical oxidation (mean ± standard deviation)

Tar ball	O:C	H:C	N:C	m/z>100 fraction	density
Fresh	0.25±0.01	1.55±0.01	0.012±0.002	0.32	1.24±0.01
O_0.7	0.32±0.01	1.59±0.01	0.012±0.000	0.28	1.24±0.01
O_1.7	0.35±0.01	1.60±0.01	0.009±0.002	0.24	1.24±0.01
O_3.9	0.35±0.01	1.59±0.01	0.010±0.003	0.24	1.24±0.01
O_6.7	0.38±0.01	1.62±0.03	0.011±0.001	0.21	1.24±0.01
N_0.5	0.37±0.01	1.57±0.02	0.012±0.001	0.25	1.25±0.01
N_2.0	0.41±0.01	1.58±0.01	0.015±0.004	0.25	1.26±0.01

15. Detailed mass spectra changes for tar ball upon 6.7 EAD photochemical aging

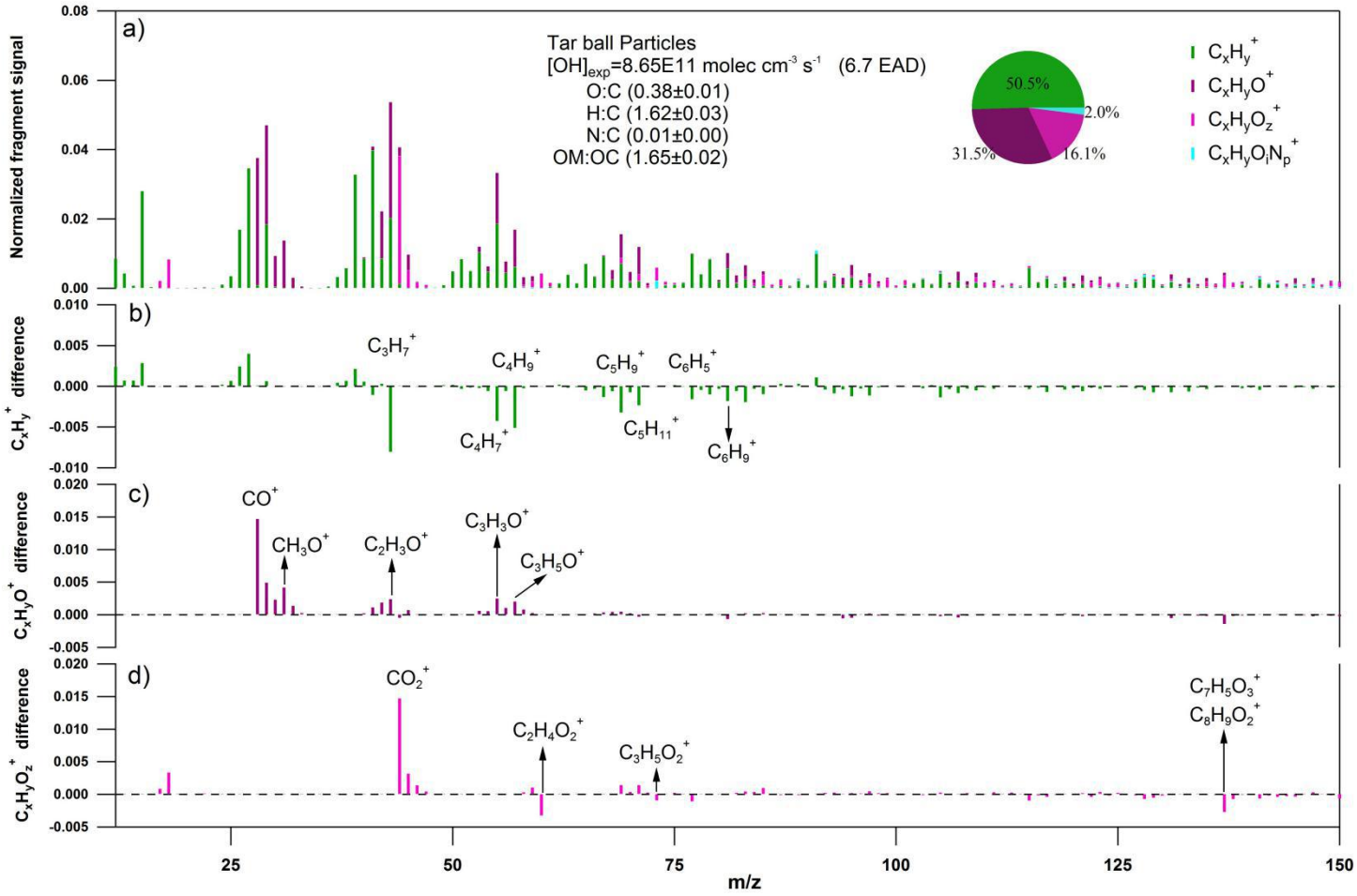

Figure S19. High-resolution mass spectral changes for nonpolar tar ball particles upon 6.7 EAD photochemical oxidation in absence of NOx. Four ion groups were grouped for clarity: $C_xH_y^+$, $C_xH_yO^+$, $C_xH_yO_z^+$ (z>1), $C_xH_yO_iN_p^+$(i≧0,p≧1). Ions O^+, OH^+, and H_2O^+ were included in the $C_xH_yO_z^+$ group. Mass fraction of the four fragment groups was pie-chart presented. a) normalized mass spectra of 6.7 EAD aged tar ball particles, b)~d) changes of $C_xH_y^+$, $C_xH_yO^+$, $C_xH_yO_z^+$, and $C_xH_yO_iN_p^+$ comparing with fresh tar ball normalized mass spectra

16. Standard AMS spectra for inorganic salt of NH_4NO_3

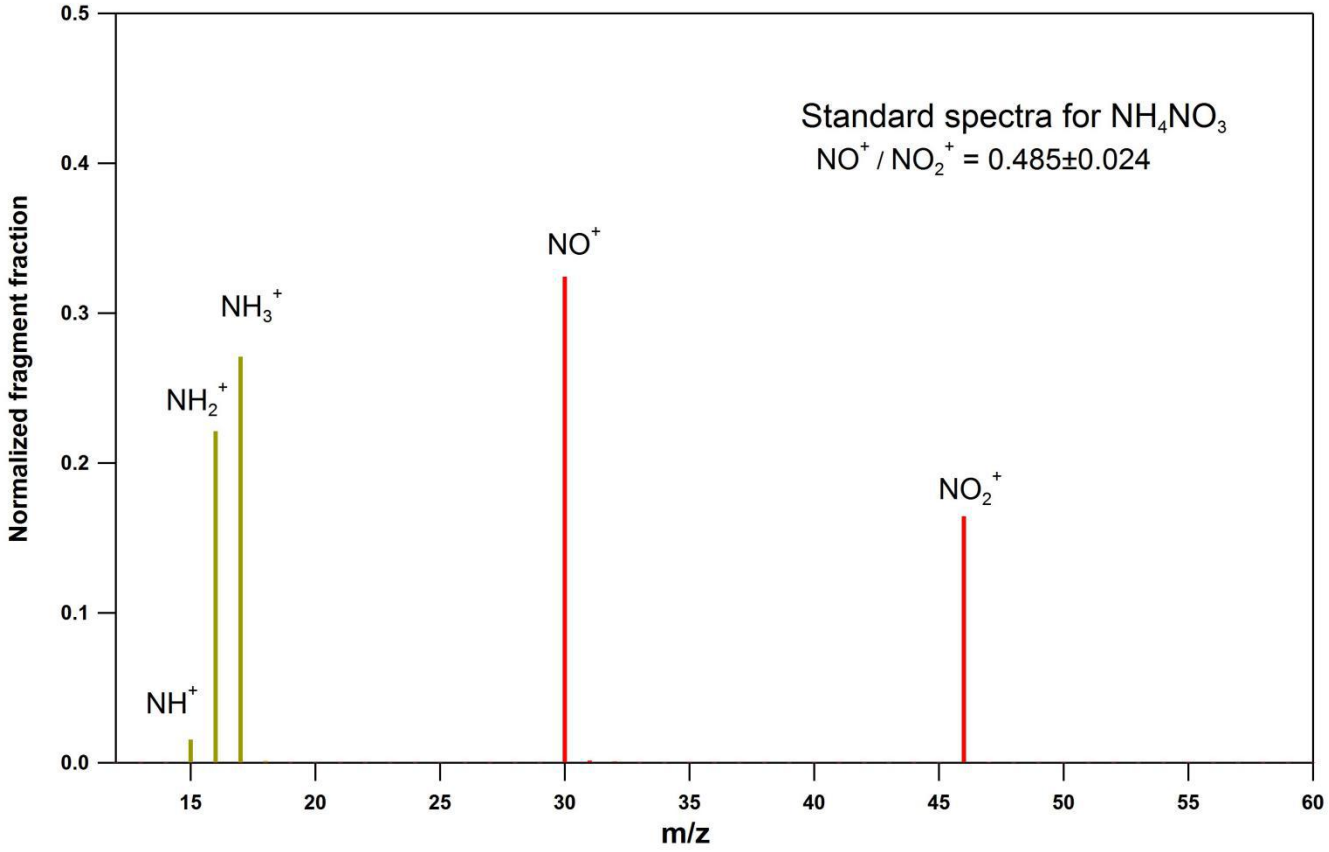

Figure S20. Standard mass spectra for NH_4NO_3 measured using HR-Tof-AMS system: NO^+ and NO_2^+ for nitrate, NH^+, NH_2^+, and NH_3^+ for ammonium

17. Detailed mass spectra changes for tar ball aerosols upon 4 EAD photochemical aging with 2.0 vol.% N_2O addition

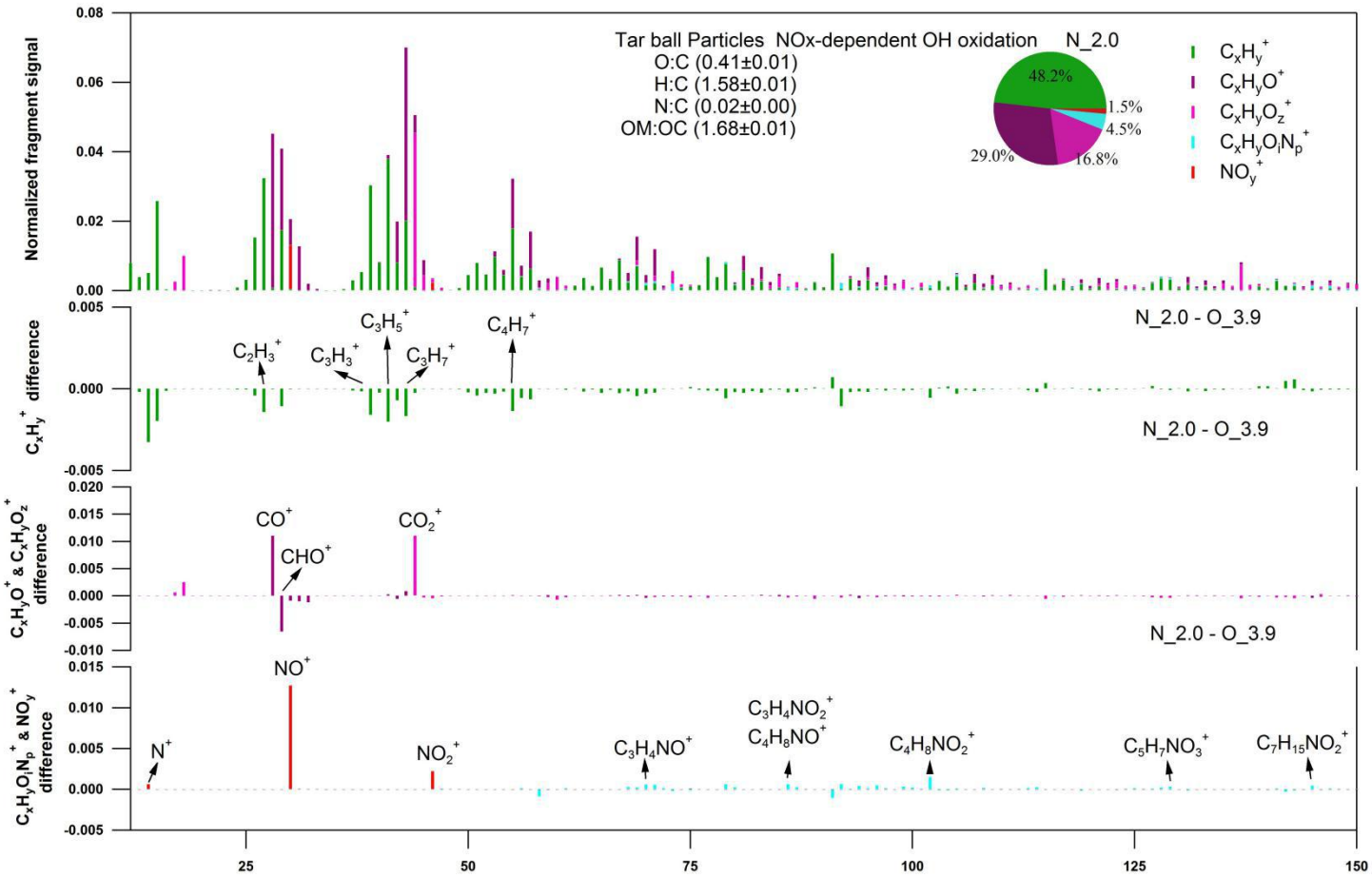

Figure S21. High-resolution mass spectra changes for nonpolar tar ball particles upon photochemical oxidation in presence of NOx, five ion groups were grouped for clarity as: $C_xH_y^+$, $C_xH_yO^+$, $C_xH_yO_z^+$ ($z>1$), $C_xH_yO_iN_p^+$($i\geqq0$,$p\geqq1$), and NO_y^+ (NO^+ and NO_2^+). Ions O^+, OH^+, and H_2O^+ were included in the $C_xH_yO_z^+$ group. Mass fraction of the four fragment groups was pie-chart presented. a) normalized mass spectra of aged tar ball particles, b)~d) changes of $C_xH_y^+$, $C_xH_yO^+$, $C_xH_yO_z^+$, $C_xH_yO_iN_p^+$, and NO_y^+ comparing with photochemical oxidized tar ball in absence of NO_x

18. Mass absorption cross section (MAC) for tar ball aerosols upon various NOx-dependent photochemical aging processes

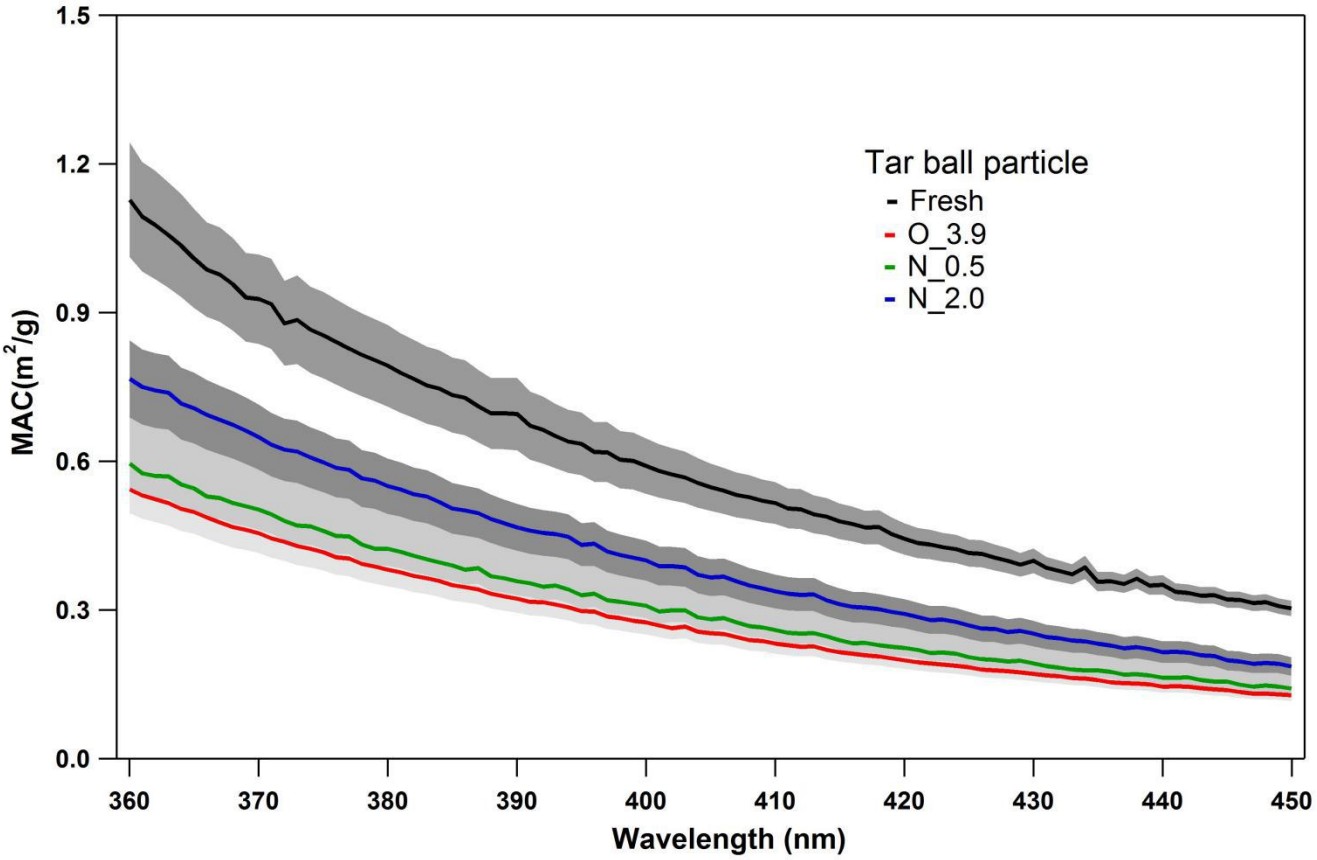

Figure S22. Mass absorption cross section (MAC) for tar ball upon NOx-dependent photochemical oxidation as a function of wavelength

19. Particle size- and light wavelength-resolved radiative forcing for tar ball aerosols oxidized via various NOx-dependent oxidation processes

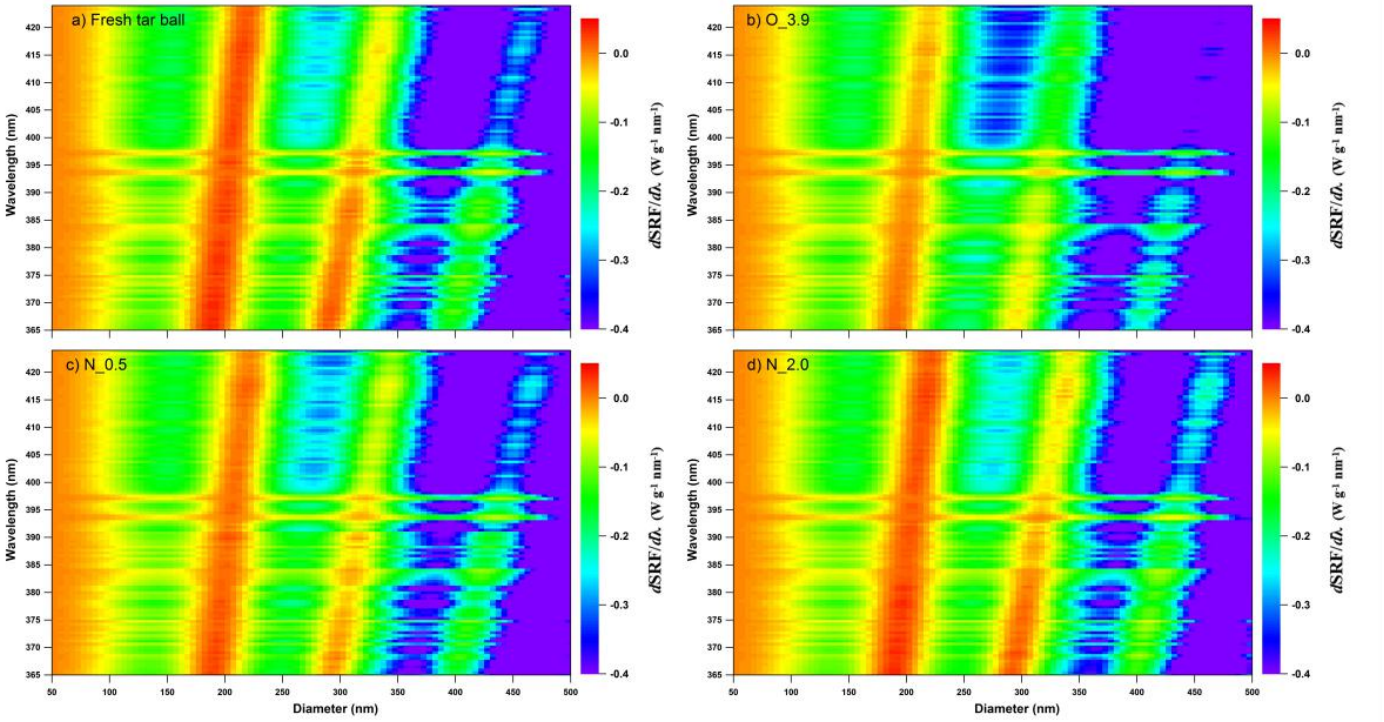

Figure S23. Ground based size-resolved radiative forcing spectra over solar irradiation of 365~425 nm for tar ball under various oxidation: a) fresh tar ball, b) 3.9 EAD daytime photochemical oxidized tar ball, c) photooxidized tar ball with 0.5 vol.% N_2O addition, d) photooxidized tar ball with 2.0 vol.% N_2O addition.

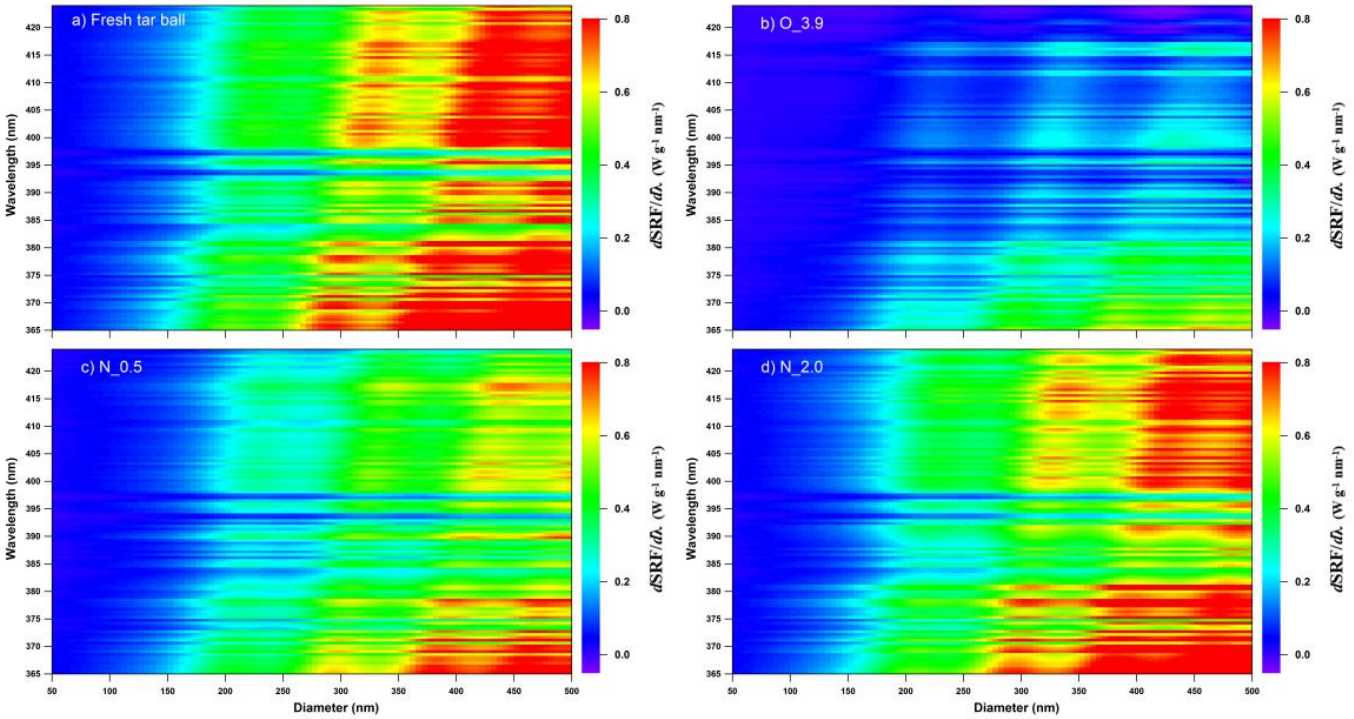

Figure S24. Snow based size-resolved radiative forcing spectra over solar irradiation of 365~425 nm for tar ball under various oxidation: a) fresh tar ball, b) 3.9 EAD OH initiated photochemical oxidized tar ball, c) photooxidized tar ball with 0.5 vol.% N_2O addition, d) photooxidized tar ball with 2.0 vol.% N_2O addition.

Reference

Adler, G., Flores, J. M., Abo Riziq, A., Borrmann, S., and Rudich, Y.: Chemical, physical, and optical evolution of biomass burning aerosols: a case study, Atmos. Chem. Phys., 11, 1491-1503, doi:10.5194/acp-11-1491-2011, 2011.

Aiken, A. C., Decarlo, P. F., Kroll, J. H., Worsnop, D. R., Huffman, J. A., Docherty, K. S., Ulbrich, I. M., Mohr, C., Kimmel, J. R., and Sueper, D.: O:C and OM/OC ratios of primary, secondary, and ambient organic aerosols with high-resolution time-of-flight aerosol mass spectrometry, Environ. Sci. Technol., 42, 4478-4485, doi: 10.1021/es703009q, 2008.

Aiona, P. K., Luek, J. L., Timko, S. A., Powers, L., Gonsior, M., and Nizkorodov, S. A.: Effect of Photolysis on Absorption and Fluorescence Spectra of Light-Absorbing Secondary Organic Aerosols, ACS Earth Space Chem., 2, 235-245, doi:10.1021/acsearthspacechem.7b00153, 2018.

Bateman, A. P., Nizkorodov, S. A., Laskin, J., and Laskin, A.: Photolytic processing of secondary organic aerosols dissolved in cloud droplets, Phys. Chem. Chem. Phys., 13, 12199-12212, doi:10.1039/C1CP20526A, 2011.

Bente, M., Sklorz, M., Streibel, T., and Zimmermann, R.: Online laser desorption-multiphoton postionization mass spectrometry of individual aerosol particles: molecular source indicators for particles emitted from different traffic-related and wood combustion sources, Anal. Chem., 80, 8991-9004, doi: 10.1021/ac801295f, 2008.

Bruns, E., Krapf, M., Orasche, J., Huang, Y., Zimmermann, R., Drinovec, L., Močnik, G., El-Haddad, I., Slowik, J., and Dommen, J.: Characterization of primary and secondary wood combustion products generated under different burner loads, Atmos. Chem. Phys., 15, 2825-2841, doi:10.5194/acp-15-2825-2015, 2015.

Chýlek, P., Ramaswamy, V., and Cheng, R. J.: Effect of graphitic carbon on the albedo of clouds, J. Atmos. Sci., 41, 3076-3084, doi:10.1175/1520-0469, 1984.

d'Almeida, G. A., Koepke, P., and Shettle, E. P.: Atmospheric aerosols: global climatology and radiative characteristics, A. Deepak Publishing, Hampton, Va, 1991.

Epstein, S. A., Blair, S. L., and Nizkorodov, S. A.: Direct photolysis of α-pinene ozonolysis secondary organic aerosol: effect on particle mass and peroxide content, Environ. Sci. Technol., 48, 11251-11258, doi:10.1021/es502350u, 2014.

He, L. Y., Lin, Y., Huang, X. F., Guo, S., Xue, L., Su, Q., Hu, M., Luan, S. J., and Zhang, Y. H.: Characterization of high-resolution aerosol mass spectra of primary organic aerosol emissions from Chinese cooking and biomass burning, Atmos. Chem. Phys., 10, 11535-11543, doi:10.5194/acp-10-11535-2010, 2010.

Henry, K. M., and Donahue, N. M.: Photochemical aging of α-pinene secondary organic aerosol: effects of OH radical sources and photolysis, J. Phys. Chem. A, 116, 5932-5940, doi:10.1021/jp210288s, 2012.

Hoffmann, D., Iinuma, Y., and Herrmann, H.: Development of a method for fast analysis of phenolic molecular markers in biomass burning particles using high performance liquid chromatography/atmospheric pressure chemical ionisation mass spectrometry, J. Chromatography A, 1143, 168-175, doi:10.1016/j.chroma.2007.01.035, 2007.

Jacobson, M. Z.: Analysis of aerosol interactions with numerical techniques for solving coagulation, nucleation, condensation, dissolution, and reversible chemistry among multiple size distributions, J. Geophys. Res.-Atmos., 107, D19, 4366, doi:10.1029/2001JD002044, 2002.

Jacobson, M. Z.: Effects of externally-through-internally-mixed soot inclusions within clouds and precipitation on global climate, J. Phys. Chem. A, 110, 6860-6873, doi:10.1021/jp056391r, 2006.

Lee, H. J., Aiona, P. K., Laskin, A., Laskin, J., and Nizkorodov, S. A.: Effect of solar radiation on the optical properties and molecular composition of laboratory proxies of atmospheric brown carbon, Environ. Sci. Technol., 48, 10217-10226, doi: 10.1021/es502515r, 2014.

Li, C., Hu, Y., Zhang, F., Chen, J., Ma, Z., Ye, X., Yang, X., Wang, L., Tang, X., and Zhang, R.: Multi-pollutant emissions from the burning of major agricultural residues in China and the related health-economic effects, Atmos. Chem. Phys., 17, 4957-4988, doi: doi:10.5194/acp-17-4957-2017, 2017.

Li, Y., Huang, D., Cheung, H. Y., Lee, A., and Chan, C. K.: Aqueous-phase photochemical oxidation and direct photolysis of vanillin-a model compound of methoxy phenols from biomass burning, Atmos. Chem. Phys., 14, 2871-2885, doi:10.5194/acp-14-2871-2014, 2014.

Li, Y. J., Yeung, J. W., Leung, T. P., Lau, A. P., and Chan, C. K.: Characterization of organic particles from incense burning using an aerodyne high-resolution time-of-flight aerosol mass spectrometer, Aerosol Sci. Tech., 46, 654-665, doi:10.1080/02786826.2011.653017, 2012.

Liu, J., Lin, P., Laskin, A., Laskin, J., Kathmann, S. M., Wise, M., Caylor, R., Imholt, F., Selimovic, V., and Shilling, J. E.: Optical properties and aging of light-absorbing secondary organic aerosol, Atmos. Chem. Phys., 16, 12815-12827, doi:10.5194/acp-16-12815-2016, 2016.

Malecha, K. T., and Nizkorodov, S. A.: Photodegradation of secondary organic aerosol particles as a source of small, oxygenated volatile organic compounds, Environ. Sci. Technol., 50, 9990-9997, doi:10.1021/acs.est.6b02313, 2016.

Mandalakis, M., Gustafsson, Ö., Alsberg, T., Egebäck, A. L., Reddy, C. M., Xu, L., Klanova, J., Holoubek, I., and Stephanou, E. G.: Contribution of biomass burning to atmospheric polycyclic aromatic hydrocarbons at three European background sites, Environ. Sci. Technol., 39, 2976-2982,doi:10.1021/es048184v, 2005.

Mang, S. A., Henricksen, D. K., Bateman, A. P., Andersen, M. P. S., Blake, D. R., and Nizkorodov, S. A.: Contribution of carbonyl photochemistry to aging of atmospheric secondary organic aerosol, J. Phys. Chem. A, 112, 8337-8344, doi:10.1021/jp804376c, 2008.

Ng, N., Canagaratna, M., Zhang, Q., Jimenez, J., Tian, J., Ulbrich, I., Kroll, J., Docherty, K., Chhabra, P., and Bahreini, R.: Organic aerosol components observed in Northern Hemispheric datasets from Aerosol Mass Spectrometry, Atmos. Chem. Phys., 10, 4625-4641, doi:10.5194/acp-10-4625-2010, 2010.

Ng, N., Canagaratna, M., Jimenez, J., Chhabra, P., Seinfeld, J., and Worsnop, D.: Changes in organic aerosol composition with aging inferred from aerosol mass spectra, Atmos. Chem. Phys., 11, 6465-6474, doi:10.5194/acp-11-6465-2011, 2011.

Norrish, R. G.: Part II. Free radicals of short life: chemical aspects. A. General and inorganic. The primary photochemical production of some free radicals, Transactions of the Faraday Society, 30, 103-113, 1934.

Passig, J., Schade, J., Oster, M., Fuchs, M., Ehlert, S., Jäger, C., Sklorz, M., and Zimmermann, R.: Aerosol mass spectrometer for simultaneous detection of polyaromatic hydrocarbons and inorganic components from individual particles, Anal. Chem., 89, 6341-6345, doi:10.1021/acs.analchem.7b01207, 2017.

Pitts, J., Wan, J., and Schuck, E.: Photochemical studies in an alkali halide matrix. I. An o-nitrobenzaldehyde actinometer and its application to a kinetic study of the photoreduction of benzophenone by benzhydrol in a pressed potassium bromide disk, J. Am. Chem. Soc., 86, 3606-3610, 1964.

Samburova, V., Connolly, J., Gyawali, M., Yatavelli, R. L., Watts, A. C., Chakrabarty, R. K., Zielinska, B., Moosmüller, H., and Khlystov, A.: Polycyclic aromatic hydrocarbons in biomass-burning emissions and their contribution to light absorption and aerosol toxicity, Sci. Total Environ., 568, 391-401, doi:10.1016/j.scitotenv.2016.06.026, 2016.

Santos, G. T., Santos, P. S., and Duarte, A. C.: Vanillic and syringic acids from biomass burning: Behaviour during Fenton-like oxidation in atmospheric aqueous phase and in the absence of light, J. Hazard. Mater., 313, 201-208, doi:10.1016/j.jhazmat.2016.04.006, 2016.

Sedlacek III, A. J., Buseck, P. R., Adachi, K., Onasch, T. B., Springston, S. R., and Kleinman, L.: Formation and evolution of Tar Balls from Northwestern US wildfires, Atmos. Chem. Phys., 18, 11289-11301, doi:10.5194/acp-18-11289-2018, 2018.

Sumlin, B. J., Pandey, A., Walker, M. J., Pattison, R. S., Williams, B. J., and Chakrabarty, R. K.: Atmospheric Photooxidation Diminishes Light Absorption by Primary Brown Carbon Aerosol from Biomass Burning, Environ. Sci. Technol. Lett., 4, 540-545, doi:10.1021/acs.estlett.7b00393, 2017.

Sumlin, B. J., Oxford, C. R., Seo, B., Pattison, R. R., Williams, B. J., and Chakrabarty, R. K.: Density and homogeneous internal composition of primary brown carbon aerosol, Environ. Sci. Technol., 52, 3982-3989, doi: 10.1021/acs.est.8b00093, 2018.

Takahama, S., Johnson, A., Morales, J. G., Russell, L. M., Duran, R., Rodriguez, G., Zheng, J., Zhang, R., Toom-Sauntry, D., and Leaitch, W. R.: Submicron organic aerosol in Tijuana, Mexico, from local and Southern California sources during the CalMex campaign, Atmos. Environ., 70, 500-512, doi:10.1016/j.atmosenv.2012.07.057, 2013.

Tang, I. N.: Thermodynamic and optical properties of mixed-salt aerosols of atmospheric importance, J. Geophys. Res. Atmos., 102, 1883-1893, doi:10.1029/96JD03085, 1997.

Veres, P., Roberts, J. M., Burling, I. R., Warneke, C., de Gouw, J., and Yokelson, R. J.: Measurements of gas-phase inorganic and organic acids from biomass fires by negative-ion proton-transfer chemical-ionization mass spectrometry, J. Geophys. Res. Atmos., 115, doi:10.1029/2010JD014033, 2010.

Wong, J. P., Nenes, A., and Weber, R. J.: Changes in light absorptivity of molecular weight separated brown carbon due to photolytic aging, Environ. Sci. Technol., 51, 8414-8421,doi:10.1021/acs.est.7b01739, 2017.

Wong, J. P., Zhou, S., and Abbatt, J. P.: Changes in secondary organic aerosol composition and mass due to photolysis: relative humidity dependence, J. Phys. Chem. A, 119, 4309-4316, doi: 10.1021/jp506898c, 2014.

Yee, L., Kautzman, K., Loza, C., Schilling, K., Coggon, M., Chhabra, P., Chan, M., Chan, A., Hersey, S., and Crounse, J.: Secondary organic aerosol formation from biomass burning intermediates: phenol and methoxyphenols, Atmos. Chem. Phys., 13, 8019-8043, doi:10.5194/acp-13-8019-2013, 2013.

Zhou, S., Collier, S., Jaffe, D. A., Briggs, N. L., Hee, J., Sedlacek III, A. J., Kleinman, L., Onasch, T. B., and Zhang, Q.: Regional influence of wildfires on aerosol chemistry in the western US and insights into atmospheric aging of biomass burning organic aerosol, Atmos. Chem. Phys., 17, 2477-2493, doi: 10.5194/acp-17-2477-2017, 2017.